(Article begins on next page)

1   **A novel role for CRIM1 in the corneal response to UV and pterygium development**

2   Eleonora Maurizi[1], Davide Schiroli[1], Sarah D. Atkinson[1,2], Laura Mairs[1], David G. Courtney[1],

3   Barry O'Hagan[1], Victoria E. McGilligan[1,2], Alastair T. Pagnamenta[3], Jenny C. Taylor[3], Jesus J.D.

4   Vasquez[4], Daniel E. Illanes-Velarde[4], Dave Goldsmith[5], Pieter Gouws[6], Jonathan E. Moore[1], M.

5   Andrew Nesbit[1*], C.B. Tara Moore[1*].

6   **Affiliations**

7   [1] Biomedical Sciences Research Institute, Ulster University, Coleraine, Northern Ireland, BT52

8   1SA, UK.

9   [2] Northern Ireland Centre for Stratified Medicine, Biomedical Sciences Research Institute, C-TRIC

10 Building, Altnagelvin Area Hospital, Ulster University, Derry/Londonderry, BT47 6SB, UK.

11 [3] Wellcome Trust Centre for Human Genetics, University of Oxford, Oxford, UK.

12 [4] Facultad de Medicina, Santa Cruz de la Sierra, Santa Cruz, Bolivia.

13 [5] Andean Medical Mission, 42, Sherwood Road, Bognor Regis, West Sussex, PO22 9DR, UK.

14 [6] Conquest Hospital, The Ridge, St Leonards-on-Sea, East Sussex, TN37 7RD, UK.

15

16 * To whom correspondence should be addressed: Biomedical Sciences Research Institute,

17 University of Ulster, Coleraine, Northern Ireland BT52 1SA, United Kingdom. Tel no:

18 +44(0)2870124577. Fax no: +44(0)28703324915. Email: a.nesbit@ulster.ac.uk,

19 t.moore@ulster.ac.uk.

20 The authors wish it to be known that, in their opinion, the last two authors should be regarded as co-

21 corresponding authors.

22

23

24

25 **ABSTRACT**

26 Pterygium is a pathological proliferative condition of the ocular surface, characterized by formation

27 of a highly vascularized, fibrous tissue arising from the limbus that invades the central cornea leading

28 to visual disturbance and, if untreated, blindness. Whilst chronic ultraviolet (UV) light exposure plays

29 a major role in its pathogenesis, higher susceptibility to pterygium is observed in some families,

30 suggesting a genetic component.

31 In this study, a Northern Irish family affected by pterygium but reporting little direct exposure to UV

32 was identified carrying a missense variant in *CRIM1* NM_016441.2: c.1235 A>C (H412P) through

33 whole-exome sequencing and subsequent analysis. *CRIM1* is expressed in the developing eye, adult

34 cornea and conjunctiva, having a role in cell differentiation and migration but also in angiogenesis,

35 all processes involved in pterygium formation. We demonstrate elevated *CRIM1* expression in

36 pterygium tissue from additional individual Northern Irish patients compared to unaffected

37 conjunctival controls.

38 UV irradiation of HCE-S cells resulted in an increase in ERK phosphorylation and *CRIM1* expression,

39 the latter further elevated by the addition of the MEK1/2 inhibitor, U0126. Conversely, siRNA

40 knockdown of *CRIM1* led to decreased UV-induced ERK phosphorylation and increased *BCL2*

41 expression.

42 Transient expression of the mutant H412P *CRIM1* in corneal epithelial HCE-S cells showed that,

43 unlike wild-type *CRIM1*, it was unable to reduce the cell proliferation, increased ERK

44 phosphorylation and apoptosis induced through a decrease of *BCL2* expression levels.

45 We propose here a series of intracellular events where *CRIM1* regulation of the ERK pathway

46 prevents UV-induced cell proliferation and may play an important role in the in the pathogenesis of

47 pterygium.

48

49   **Keywords:** CRIM1; pterygium; UV; proliferation; ERK; apoptosis; variant

50

51   **Abbreviations: BCL2**, B-cell lymphoma 2; **BMP,** Bone Morphogenetic Proteins; **CRIM1**, Cysteine Rich Motoneuron protein1; **EMT,** Epithelial

52   mesenchymal transition; **ERK (I)**, Extracellular signal–regulated kinases (Inhibitor); **HCE-S**, Human Corneal Epithelial cells; **IC,** Impression

53   Cytology; **IGV,** Integrative Genomic Viewer; **MAF,** Minor allele frequency; **MAPK**, Mitogen-activated protein kinases; **MTT,** 3-(4,5-

54   dimethylthiazol-2-yl)-2,5-diphenyltetrazolium bromide; **NGS,** Next Generation sequencing; **NI,** Northern Irish; **PolyPhen,** Polymorphism

55   Phenotyping; **SIFT**, Sorting Intolerant From Tolerant**; TiGER,** Tissue-specific Gene Expression and Regulation; **TGF-β (I)**, Transforming Growth

56   Factor- β (Induced); **TUNEL,** Terminal deoxynucleotidyl transferase dUTP nick end labelling; **VEGFA,** Vascular Endothelial Growth FactorA;

57   **VW(F)-C,** Von Willebrand (Factor) C; **WES,** Whole Exome Sequencing.

58

1. INTRODUCTION

Pterygium (OMIM 178000) is a triangular shaped proliferative fibrovascular growth arising from the corneal-scleral limbus that invades the cornea centripetally[1,2]. The corneal invasion, through an active process of cell proliferation, matrix remodelling, angiogenesis and inflammation[1,3], results in astigmatism, irritation, tearing, and, if the visual axis is impinged upon, blindness in the most severe cases[4]. The only effective treatment for pterygium is surgical excision which, together with various adjuvant therapies, still presents a 12% recurrence rate[5]. A small conjunctival lesion, pinguecula, is considered to be related to pterygium with a similar aetiology[6], limbal localisation[7] and histology[8].

The main trigger for pterygium has long been attributed to UV radiation[9-11], with epidemiologic studies showing an average prevalence of 22% (as high as 40% in some Chinese populations[12] or 45% in provincial Indonesia[13]) in the "pterygium belt", an equatorial zone between latitudes 40°N and 40°S, compared to only 2% outside this area[4]. The human cornea represents a shield to protect the anterior eye from UV light and its anisotropic properties ensure that UV transmittance is reduced with a lower wavelength: while UVB (290-320nm) is completely absorbed by corneal epithelium, UVA (320-400nm) is absorbed only by 20% by the epithelial layer with the rest reaching the underlying stroma[14]. Focussing of incident light upon the nasal limbus has been proposed as the mechanism for the more frequent occurrence of pterygia at this location[15].

In pterygium, while UVB mediates oxidative DNA damage[16,17] and induction of cytokines and growth factors[18], both UVB[19] and UVA[20] are responsible for activation of ERK intracellular pathway.

Irritation and chronic inflammation caused by sand, dust and wind[21], as well as viral infections[22,23], have been suggested as additional environmental triggers for pterygium.

A genetic contribution to the incidence of pterygium was suggested in an Australian study[24], which revealed that 38% of patients admitted to hospital for excision of pterygia reported relatives

4

84   with the disease, and in studies where different ethnic groups living at the same geographical

85   location display differing prevalence of pterygium[12,25].

86   High incidence of pterygium has been reported in a number of multigenerational families[26,27] and

87   in monozygotic twins[28,29], where the most commonly reported mode of inheritance is autosomal

88   dominant with reduced penetrance[4,30,31].

89   The lack of large families presenting with multiple affected individuals, compounded by the late-

90   onset of the disease, together with incomplete penetrance, has hampered identification of

91   causative genes for pterygium.

92   Candidate gene association studies, which derive from hypotheses in which the cause of

93   pterygium is already assumed, have identified an increased predisposition to pterygium in

94   individuals carrying germline mutations in genes related to: oxidative stress[16,32], carcinogenesis[33]

95   or angiogenesis[34]; even though these analyses have been found subject to false-positive

96   associations[35]. Next-generation sequencing techniques, such as Whole Exome Sequencing (WES)

97   and Whole Genome Sequencing (WGS), provide a largely hypothesis-free approach to identifying

98   causative genes in smaller families with fewer affected members[36].

99   In this study, using a WES approach, combined with bioinformatic and functional analysis, we

100   identified a missense variant, p.His412Pro, in the *CRIM1* (cysteine rich motor neuron protein 1)

101   gene, found in pterygium affected members of large multigenerational Northern Irish family with

102   a documented small exposure to sunlight. *CRIM1* response to UV exposure revealed, for the first

103   time, a central role within an intracellular mechanism involving ERK phosphorylation and

104   ultimately leading to cellular proliferation or apoptosis. Introduction of the H412P variant in

105   *CRIM1* resulted in an impairment of the whole pathway, demonstrating its possible involvement

106   in the NI family's pterygium pathogenesis.

107

108

2. MATERIALS AND METHODS

2.1 Patient clinical examination

Clinical examinations were performed at Cathedral Eye Clinic, Belfast, UK (pterygium family members, pterygium and control individual samples from Northern Ireland).

A total of 24 patients from three consecutive generations of a Caucasian Northern Irish family affected by pterygium were investigated: three with pterygium, two with pinguecula and one unaffected family member participated to the WES study. Additional Northern Irish and Bolivian individuals (pterygium affected and unaffected controls) were recruited for sequence analysis of *CRIM1* and *CRIM1* expression analysis.

Following informed consent, collection of blood, tissues and a completed questionnaire was obtained from each participating individual under ethical approval from ORECNI Northern Ireland, UK (09/NIR01/14) and Comité de Bioética de la Facultad de Medicina, Santa Cruz, Bolivia.

2.2 Whole Exome Sequencing and Ingenuity Variant Analysis

WES was performed at the Wellcome Trust Centre for Human Genetics, University of Oxford. Briefly, genomic DNA was extracted from blood leukocytes using the QIAamp DNA Blood mini kit (QIAGEN, Manchester, UK), quantified by the high sensitivity Qubit system (Thermo Fisher Scientific, Loughborough, UK) and integrity of the DNA confirmed by electrophoresis on a 1% agarose gel.

The SureSelect Human All Exon v2 kit was used for Whole Exome capture according to the manufacturer's instructions (Agilent Technologies UK, Wokingham, Berkshire, UK). The SureSelect n.2100 Bioanalyser (Agilent Technologies) allowed an assessment of the quality of the exome enriched library obtained.

132   Parallel sequencing was then performed by Illumina GAIIx using 150bp-paired-end reads.

133   Generated reads were aligned to the Human 37 reference genome with a short read mapper

134   (Stampy) generating data in BAM format[37].

135   Coverage of the target region was verified to be in excess of 70% (greater than 10 reads). Platypus,

136   an in-house variant caller able to detect Single Nucleotide Variants (SNVs) and short (<50bp)

137   insertion/deletions (INDEL), was used to detect variant sites and alleles. Once the false positive

138   rate was reduced, the resulting variants were stored as Variant Call Format (VCF) files. Ingenuity

139   Variant analysis (Qiagen) was used to filter and select a smaller number of candidate genes.

140   Aligned WES reads were viewed with the IGV platform. Clustal X2.1 was used to align CRIM1

141   sequences and results were visualized with EsPript 3.0 (http://espript.ibcp.fr)[38].

142   *2.3 Sanger Sequencing*

143   Sanger sequencing was performed on genomic DNA extracted from the blood leukocytes using

144   QIAamp DNA Blood mini kit.

145   Presence of H412P in *CRIM1* was verified using the following primers: CRIM1_F:

146   CTTCTTTTGCATGCACCCCC and CRIM1_R: TCACATGTGCAACCTTTCCTC while

147   *CRIM1* VWFs were sequenced using genomic primers designed using Primer3[39] (Supplementary

148   Table2). The PCR products were verified on a 1% agarose gel and Sanger sequenced at the

149   Department of Zoology, University of Oxford.

150   *2.4 Tissues and Impression cytology samples*

151   Tissues samples (pterygium and normal cornea) were collected during surgeries while impression

152   cytology samples were obtained using 4 x 4 mm strips of sterile LCR biopore membrane filter

153   (pore size, 0.45 um; Millipore, Watford, UK) post pterygium surgery as previously described[40]

154   and stored in RNAlater (Qiagen). Prior to IHC staining tissues were fixed in 95% ethanol for 20

155   minutes at room temperature. The RNA yield obtained from the impression cytology samples was

156   never lower than 8ng/ul and never higher than 15ng/ul. The ratio of absorbance at 260 and 280

7

157 nm (A260/280) of the RNA samples was between 1.8 and 2.2. Samples for which the RNA yield

158 was too low or the quality fell outside the limits were excluded.

159

160 ## 2.5 Quantitative real-time PCR

161 RNA extracted using the RNeasy Plus Mini Kit (Qiagen, Manchester, UK) was quantified with

162 the Nanodrop 1000 (Thermo Fisher Scientific) and 1 µg of total RNA was reverse transcribed

163 into cDNA using the High Capacity cDNA Reverse Transcription Kit (Life Technologies, Paisley,

164 UK). cDNA was used for qRT-PCR assays, performed using a Lightcycler 480 II (Roche, West

165 Sussex UK).

166 Real Time Ready Assays for *CRIM1* (assay id. 112278), *VEGFA* (assay id. 140396), *SRCAP*

167 (assay id. 126413), *TGF-βI* (assay id. 104720), Glyceraldehyde 3-phosphate dehydrogenase

168 *(GAPDH)* (assay id. 141139) and hypoxanthine phosphoribosyltransferase *(HPRT)* (assay id.

169 102079) were purchased from Roche (Burgess Hill, West Sussex, UK).

170 SYBR green (Fermentas, Cambridge, UK) technology qRT-PCR was performed using *BCL2*

171 primers (For AGCATGGGAGCCACGACCCT, Rev GGCCAAGGCCACACAGCCAA) and

172 HPRT primers (For AGCTTGCGACCTTGACCAT, Rev GACCACTCAACAGGGGACAT), a

173 kind gift from H. Nesbitt[41].

174 Data were normalised using *HPRT* and *GAPDH* as housekeeping controls for ΔCt and ΔΔCt

175 calculations[42]. *HPRT* and *GAPDH* were chosen as they have been shown to be the most stable

176 corneal housekeeping genes[43]. For each condition all complementary cDNA samples were run in

177 duplicate in two independent experiments.

178 ## 2.6 HCE-S culture

179 Human Corneal Epithelial cells (HCE-S), a spontaneously generated corneal cell line[44] (a kind

180 gift from Prof. Julie Daniels), were cultured (37°C, 5% CO_2) in Dulbecco's modified Eagle's

181   medium (DMEM) containing 4 g/L glucose (Thermo Fisher Scientific, UK), and supplemented

182   with 10% fetal bovine serum (Thermo Fisher Scientific, UK).

183   *2.7 TUNEL assay*

184   The terminal deoxynucleotidyl transferase dUTP nick end labelling (TUNEL) assay was

185   performed on HCE-S cells which had been reverse transfected with Lipofectamine 2000 using a

186   mock transfection with pGL4.17 [luc2/Neo] plasmid (Promega Madison, WI USA), *CRIM1* wild

187   type or *CRIM1* H412P plasmids. After 72 hours cells were fixed with 4% paraformaldehyde

188   (PFA) and stained using the In Situ Cell Death Detection kit (Fluorescein; Roche, Burgess Hill,

189   Surrey, UK) following the manufacturer's instructions. Images were obtained using a fluorescent

190   AxioScope A1 microscope equipped with an AxioCam MRc camera (Carl Zeiss, Germany); 10x

191   objective. Twelve images for each condition (n=3) were quantified using ImageJ software (US

192   National Institutes of Health) and then normalised to total DAPI cells in each field.

193   *2.8 Immunohistochemistry (IHC)*

194   Pterygium and conjunctival tissues were formalin fixed and paraffin embedded. Sections of 7μm

195   were permeabilised with 0.5% Triton X-100 before staining, treated with Proteinase K solution

196   (Fisher Bioreagents, BP1700-50, 10ug/ml in PBS) and blocked with 5% goat serum (Sigma). A

197   rabbit polyclonal CRIM1 antibody (Abcam- ab189203) was incubated at 1:100, with a rabbit IgG

198   (Abcam) used as an isotype control. Secondary antibody fluorescein isothiocyanate (FITC)-

199   conjugated goat anti-rabbit IgG (Santa Cruz, USA) was used at a 1:100 dilution. Each section was

200   mounted with fluorescent mounting medium (DAKO) and imaged using a 20× N Archoplan lens

201   on an AxioScope.A1 microscope equipped with an AxioCam MRc camera (Carl Zeiss, Germany).

202   *2.9 Site Directed Mutagenesis*

203   *Human CRIM1* cloned into a pcDNA3.1 plasmid was a kind gift from Dr. L Wilkinson, Institute

204   for Molecular Bioscience, University of Queensland, Brisbane, Australia[45]. Site directed

205   mutagenesis was performed to obtain the H412P *CRIM1* clone, using the Quick Change II kit

9

206   (Agilent Technologies), following the manufacturer's instructions. The entire *CRIM1* sequence

207   was checked for integrity by Sanger Sequencing (Department of Zoology, University of Oxford),

208   primers used are listed in Supplementary Table1.

209   ### *2.10 MTT assay*

210   Reverse transfection was performed in 12 well plates using HCE-S cells with either

211   pCas9D10A_GFP (Addgene/Zhang lab), *CRIM1* wild-type or H412P plasmids with

212   Lipofectamine 2000, according to the manufacturer's instructions (Falcon #353043, BD Corning

213   Life Sciences, MA, USA). The following day cells were transferred in 96 well plates and 3-(4,5-

214   dimethylthiazol-2-yl)-2,5-diphenyltetrazolium bromide (MTT) was added to the medium.

215   Following 2 hours of incubation, the cells were resuspended in DMSO (Dimethyl sulfoxide,

216   Sigma), absorbance was measured at 570 nm using the FLUOstar Omega (BMG Labtech,

217   Aylesbury, UK) and quantified as relative percentages compared to control conditions.

218   Absorbance measurements for the MTT were taken at 24, 48, 72 and 96 hours post transfection.

219   ### *2.11 Western Blotting*

220   HCE-S cells were cultured as described above. Low cell seeding densities were used to avoid

221   cells becoming too confluent as this causes a decrease in ERK phosphorylation independent of

222   the effect of CRIM1[46,47].

223   Proteins were extracted using Complete Lysis-M (Roche Diagnostics) and proteinase inhibitor

224   (Sigma-Aldrich P8340), quantification of total protein was performed using the Bradford assay

225   (BioRad), 25μg of the extracted proteins was then resolved on a 4-12% NuPAGE® Bis-Tris

226   Precast Gels (Thermo Fisher Scientific UK) using NuPAGE® MOPS SDS Running Buffer and

227   transferred onto Amersham TM Hybond ECL membrane (GE Healthcare Life Sciences).

228   Phospho ERK (#9101) and ERK (#9102) primary antibodies (Cell Signalling) were used at

229   dilutions of 1:100 and 1:500 respectively with an overnight incubation at 4ºC. A secondary swine

230   anti-rabbit antibody (DakoCytomation, Ely, UK) was used at a 1:2000 dilution for 1 hour at room

231 temperature. Protein binding was detected by standard chemiluminescence: SuperSignal™ West

232 Pico Chemiluminescent Substrate (Thermo Fisher Scientific UK) and imaged using the G:BOX

233 transilluminator (Syngene). Quantification was performed using GeneTools image analysis

234 software: average peak values of phosphoERK were normalised against the average ERK values.

235 All the results obtained were then normalised to the transfection control.

236 *2.12 UV treatment and MEK1/2 inhibitor*

237 HCE-S cells were seeded in a 24-well plate at 1×10^5 cells per well in growth medium and left to

238 adhere overnight at 37ºC and 5% CO_2. The following day they were treated using a UVA cross-

239 linker (IROC Innocross AG, Ramsen, Switzerland) delivering a dose of 5.4 J/cm^2 as previously

240 described [48] or UVB at a final dose of 0.5 J/cm^2 through Arcadia D3 6% lamp (Arcadia, UK) with

241 an aluminium reflector at a distance of 15 cm from the cells for 34 minutes.

242 The same doses of UVA and UVB irradiation were used in experiments in which the inhibitor of

243 ERK phosphorylation (MEK1/2 inhibitor, U0126) was added to culture media an hour prior to

244 the UV treatment as previously described[20], at a concentration of 10μM.

245 After irradiation, HCE-S cells were incubated in culture medium at 37°C with 5% CO_2 and

246 harvested at 1, 6, 12, 24 and 48 hours.

247 *2.13 siRNA transfection*

248 Four different siRNAs targeting the *CRIM1* sequence (Set of 4 Upgrade: ON-TARGETplus

249 CRIM1 siRNA, LU-008492-00-0002, 2nmol, Dharmacon) were reverse transfected in HCE-S

250 cells using Lipofectamine RNAiMAX (Fisher Thermo Scientific), following the manufacturer's

251 instructions. The four siRNAs were transfected singularly or as a pool at a final concentration of

252 10nM and normalised to the results from a non-specific siRNA control (NSC4) [49]. A range of

253 different concentrations (0.2-0.5-1-10nM) of the siRNA pool reverse transfected in HCE-S cells

254 was subsequently tested.

255

11

256 *2.14 Statistical Analysis*

257 All error bars represent the standard error of the mean (SEM) calculated between sample

258 replicates of the same biological group. qRT-PCR, MTT and TUNEL assays significance was

259 estimated using a Student's t-test calculation or the Mann-Whitney U test in GraphPad Prism 5

260 software with data illustrated using Box plots (qRT-PCR in Fig.3). p value ≤ 0.05 was deemed to

261 be significant (*p value ≤ 0.05, **p value ≤ 0.01 and ***p value ≤ 0.001).

262

263 **3. RESULTS**

264 *3.1 WES analysis in a Northern Irish family affected by pterygium and pinguecula*

265 A multigenerational Northern Irish family presenting with pterygium and pinguecula, but not

266 other eye abnormalities, was examined (Fig.1A). Pterygium affected both males and females and

267 was diagnosed at an average age of 48 years. No history of unusual sun exposure was recorded

268 for any family member, suggesting a familial predisposition for development of

269 pterygium/pinguecula (Table 1).

270 Six members of this family underwent WES: three were affected by pterygium (II.2, II.4 and

271 II.14, 72, 70 and 65 years old respectively), two by pinguecula (III.5 and III.6, 48 and 46 years

272 old respectively), shown in Fig.2B, and one was unaffected (II.9, 58 years old). The other two

273 younger unaffected members of the family (III.2 and III.3, age 49 and 34) did not participate in

274 the WES but were subsequently analysed by Sanger Sequencing.

275 WES resulted in the identification of 451,153 variants in 18,858 different genes which were

276 filtered in a stepwise manner by Variant analysis software (Ingenuity®) (Fig.1C). Selecting only

277 those variants with a call quality ≥ 50 in any case and ≥ 20 in the control and a read depth ≥ 10;

278 30,000 variants were obtained. When variants with a minor allele frequency (MAF) greater than

279 0.5% (pterygium prevalence in Europe is 2%) in 1000 Genomes Project, ESP EA exomes and

12

280   Complete Genomics genome were excluded, the number of variants was reduced to 25,000.

281   Analysis using either of the two algorithms Polyphen and SIFT, predicted as deleterious 11,000

282   variants, while 40 variants were finally selected as displaying an autosomal dominant segregation

283   pattern within the family (Table 2).

284   Genes carrying mutations previously associated with pterygium such as *Ku70*, *GSTM1*, *ACE*

285   *hOGG1*[16,17,33,34] were not observed in the selected list of variants.

286   Each single variant obtained by this analysis was then manually reviewed for determination of

287   protein structure/function in Polyphen and SIFT, conservation of the amino acid among species

288   running BLAST or eye expression interrogating Tiger Expression database. Literature was

289   reviewed for any possible known correlation between gene mutations and pterygium or other

290   diseases, either of the eye or otherwise. Moreover, adequate sequencing coverage and co-

291   segregation of the variant within the family were verified through Integrative Genomic Viewer

292   (IGV) (Table 2).

293   Based on the gene expression profile and on the known role in the eye, we selected *CRIM1* as our

294   most plausible candidate gene. Recent studies have elucidated the importance of CRIM1

295   expression in corneal and conjunctival development[50-52] and the same variant, H412P, was

296   identified from another WES study on patients affected by Coloboma eye developmental

297   disorder[53]. Moreover, CRIM1 revealed a role in cell proliferation[54-56], adhesion and migration[57-

298   59], angiogenesis through VEGFA[60-62] and UV-related diseases[63,64], the main processes involved

299   in pterygium development[4].

300

301   *3.2 CRIM1 structure and sequence analysis in individuals from Northern Ireland and Bolivia.*

302   Presence of the variant in each affected family member, and absence from the unaffected sibling

303   (II.9), was confirmed by direct Sanger sequencing (Fig.2A, example) of PCR products spanning

304   the variant in VWFC-2.

13

305　　Sequence alignment of *CRIM1* orthologues revealed residue H412 being conserved throughout

306　　human (*Homo sapiens*), cattle (*Bos Taurus*), mouse (*Mus musculus*), rat (*Rattus norvegicus*), frog

307　　(*Xenopous laevis*), zebrafish (*Danio rerio*) (Fig.2B).

308　　CRIM1 is a 1002 amino acid transmembrane protein (once the 34 amino acid signal peptide has

309　　been cleaved) and consists of a large N-terminal extracellular portion composed of 11 domains

310　　(six Von Willebrand factor C, four antistasin-like and one Insulin-like Growth Factor-binding

311　　Protein (IGFBP)), a 21 amino acids transmembrane domain and a small 76 amino acid C-terminal

312　　cytoplasmic domain[65] (Fig.2C).

313　　Although H412, located in the second VWFC domain, is not conserved in the other five VWFC

314　　of *CRIM1* (Fig.2D), it is conserved in the VWFC-2 domain of human chordin and in the VWFC-

315　　2 and 3 domains of human neuralin[66], two related bone morphogenic protein (BMP) antagonists,

316　　like CRIM1, all of which have a proven role during embryogenesis[45] (Fig.2E).

317　　Sequence analysis of VWFC-2 in two additional younger family members (III.2 and III.3, age 49

318　　and 34) revealed them to possess the same H412P variant; despite these individuals not having

319　　developed any signs of the disease. This is not incompatible with the mutation predisposing to the

320　　pathology, since a pattern of reduced penetrance has been widely described in familial

321　　pterygium[1,4,26].

322　　All the CRIM1 VWFC domains are important for interaction with BMPs 4 and 7[45,67] as well as

323　　with VEGFA, TGF-β and PDGF: if any of those domains are deleted, the interaction with the

324　　TGF-β superfamily members is disrupted[62]. VEGFA, TGF-βs and PDGF have an important role

325　　in pterygium formation[3,68]: an altered interaction of those factors with CRIM1 VWFC domains

326　　could therefore have a role in pterygium development. Sanger sequencing analysis was

327　　subsequently performed for all the six VWFC domains of *CRIM1* (primers listed in

328　　Supplementary Table2) in genomic DNA obtained from two ethnically different populations: 12

329　　affected individuals from Northern Ireland and 9 from Bolivia (Table3).

14

330   While the H412P variant was found in none of the pterygium affected individuals, one patient

331   from Bolivia, B1 (Table3), presented with a cytosine to thymine transition in the first position of

332   codon 745, predicted to result in an Arginine to Cysteine (R745C) amino acid change (dbSNP:

333   rs145721446) between VWFC-4 and VWFC-5 (exon 13). Although the MAF of this variant is

334   0.000008237 (Supplementary Fig.1A) and the R745C variant is predicted to be possibly

335   damaging by PolyPhen, this arginine residue is not conserved in other species and is substituted

336   by histidine in cattle, mouse, and rat, and by serine in both frog and zebrafish (Supplementary

337   Fig.1B). The significance of this sequence variant is unclear and not explored here.

338

339   *3.3 CRIM1 expression analysis*

340   Global expression databases indicated *CRIM1* expression in the whole eye, without differentiating

341   between specific tissues. The location of CRIM1 expression in pterygium tissue and normal

342   conjunctiva from sporadic Northern Irish individuals was therefore assessed by

343   immunohistochemistry (IHC) and qRT-PCR (Fig.3).

344   CRIM1 was detected, by IHC, lengthwise across the whole pterygium tissue: from the anterior

345   head (Fig.3A) to the posterior tail (Fig.3C). Moreover, CRIM1 was observed both in the external

346   hypertrophic conjunctival epithelium and in the internal fibroblasts, in particular in the vascular

347   endothelial cells surrounding the blood vessels (Fig.3C arrows).

348   Within the pterygium stroma, CRIM1 was found around unusual structures such as hair follicles

349   and inside sebaceous glands (Fig.3B). Finally, CRIM1 was detected in normal conjunctiva

350   (Fig.3E) and in post-surgical impression cytology samples of unaffected individuals (Fig.3F).

351   *CRIM1* expression level was further investigated using qRT-PCR on RNA obtained from post-

352   surgical impression cytology samples (Fig.3F) of unrelated Northern Irish (4 pterygium and 4

353   controls) individuals, together with a sample from a Northern Irish affected family member (II.2),

354   found with the *CRIM1* H412P variant (Fig.3G).

15

355   *CRIM1* expression is significantly higher in pterygium tissues when compared to unaffected

356   conjunctival controls ($2^{-\Delta Ct}$ mean values are 4.22 ± 0.76 and 1.28 ± 0.122, while median values

357   are 3.4 and 1.3 respectively, p = 0.028). Intriguingly, *CRIM1* expression in the Northern Irish

358   family member II.2 pterygium is lower than that of the all unaffected controls from NI ($2^{-\Delta Ct}$ value

359   of 0.32).

360   Thus, we have shown that CRIM1 expression, both at the RNA and protein level, is higher in

361   pterygium than in unaffected control tissue.

362

363   *3.4 Effects of UV on CRIM1 expression in corneal epithelial (HCE-S) cells*

364   UV radiation is considered the main epidemiologic factor responsible for pterygium and

365   pinguecula development[9-11]. Although some papers state that pterygium originates from

366   conjunctiva and Tenon's fibroblasts[69], the common consensus is that the first trigger for pterygium

367   development occurs at the limbal area[1,2,70-72] and pterygium growth has often been described as a

368   localised limbal stem cell deficiency[70]. Since the aim of this paper is studying the early events

369   triggering pterygium development, we considered that the best model would be a cell line coming

370   from the zone where the initial events characterizing the disease have been described: the limbus.

371   For this reason, for *in vitro* experiments we chose the HCE-S cell line, which spontaneously

372   originated from corneal cells of the limbal area[44].

373   The effects of UV light exposure upon HCE-S cells *in vitro* were therefore investigated. The

374   average daily dose of UV light has been estimated to be 60-70 J/cm^2 in central Europe[74].

375   Considering one hour exposure daily in general population, we irradiated an HCE-S monolayer

376   to a dose of 5.4 J/cm^2 UVA[20,75], and a dose of 0.5 J/cm^2 UVB.

377   Following UVA exposure, *CRIM1* expression started increasing from 3 hours, becoming

378   significantly different from untreated control by 6 hours and continuing up to 24 hours ($2^{-\Delta\Delta Ct} \pm$

379   SEM values at 3, 6 and 24 hours are respectively: 0.90 ± 0.15, 8.59 ± 0.22 $p \leq 0.05$ and $10.39 \pm$

380 0.40 p ≤ 0.01) (Fig.4A). UVB resulted in a significant increase in *CRIM1* expression at 24 hours

381 after the treatment when compared to the untreated control ($2^{-\Delta\Delta Ct}$ ± SEM values at 3, 6 and 24

382 hours are respectively: 1.31 ± 0.03, 0.90 ± 0.01 and 1.95 ± 0.008, the last with a p ≤ 0.05). Since

383 irradiation with UVA has similar, but greater effects on *CRIM1* expression than UVB, subsequent

384 experiments were conducted using UVA alone.

385 ERK phosphorylation, previously shown to be increased in pterygium cells following UVA

386 exposure [19,20], was assessed in UVA-treated HCE-S cells as described above. This resulted in a

387 5.6-fold increase in ERK phosphorylation compared to the untreated control at 6 hours after UVA

388 treatment, rising to 32.1-fold higher at 24 hours (Fig.4B). Treatment of HCE-S cells with the

389 MEK1/2 inhibitor, U0126, prior to UVA irradiation resulted in a complete inhibition of UVA-

390 induced ERK phosphorylation.

391 Since UVA significantly elevated both *CRIM1* expression and ERK phosphorylation at 24

392 hours after treatment, the effects of inhibition of ERK phosphorylation on *CRIM1* expression

393 following UV irradiation were studied. Surprisingly, inhibition of ERK phosphorylation in HCE-

394 S cells significantly (p<0.001) potentiated the UV-induced increase in *CRIM1* expression at 24

395 hours (UVA + inhibitor: 3.75 ± 0.12, UVA only: 1.82 ± 0.15, inhibitor only 0.77 ± 0.02, untreated

396 control: 0.63 ± 0.07; values expressed as $2^{-\Delta Ct}$) (Fig.4C).

397 Several studies have shown that increased ERK activity is associated with a decreased

398 expression of the anti-apoptotic transcription factor, B*CL2* and an increased apoptosis[76].

399 Increased expression of *BCL2* and decreased expression of apoptosis markers has been observed

400 in pterygia[1,77]. With this in mind, the expression level of *BCL2* was investigated following UVA

401 treatment activating the ERK pathway in HCE-S cells.

402 Either UVA treatment or inhibition of ERK phosphorylation in HCE-S cells alone significantly

403 decreased *BCL2* expression ($2^{-\Delta\Delta Ct}$ ± SEM values for ERK-I: 0.53 ± 0.05 and UVA 0.48 ± 0.06;

404 both p ≤ 0.05) (Fig.4D). In comparison to those, when HCE-S cells were treated with MEK1/2

17

405   inhibitor, U0126, and UVA irradiation, *BCL2* expression was significantly increased ($2^{-\Delta\Delta Ct}$ ±

406   SEM of 1.45 ± 0.13; $p \leq 0.001$) and restored levels seen in untreated cells ($p = 0.06$).

407   UV irradiation has therefore a fundamental role in triggering a series of events, including the

408   increase of *CRIM1* expression and the phosphorylation of ERK, corresponding to a decrease in

409   *BCL2* levels in HCE-S cells.

410

411   *3.5 CRIM1 intracellular pathway triggered by UVA*

412   CRIM1, ERK and BCL2, as shown above, are interrelated in playing a pivotal role in the

413   intracellular pathway triggered by UV exposure in HCE-S.

414   To further investigate the relationship between those factors, we sought to assess the effects of

415   knocking down expression of *CRIM1* following siRNA transfection. Four siRNAs targeting

416   *CRIM1*, both separately and in a pool, efficiently knocked down endogenous *CRIM1* expression

417   in HCE-S cells to less than 30% of untreated level, 48 hours after transfection ($p \leq 0.001$)

418   (Supplementary Fig.2).

419   Endogenous levels of *CRIM1* expression in HCE-S, normalised to cells transfected with NSC

420   siRNA, increased after UVA treatment by 1.7 ± 0.05 fold, $p \leq 0.05$. Because levels of *CRIM1*

421   expression appear critical and finely regulated following UV irradiation, the concentration of

422   siCRIM1 was titrated (0.2nM, 0.5nM, 1nm and 10nM) to establish the concentration at which

423   *CRIM1* expression was the same as non-UVA treated, NSC4-tranfected HCE-S cells

424   (Supplementary Fig.3). The siCRIM1 concentration at which this was achieved was 0.5nM

425   (Fig.5A).

426   Since pterygium is considered a proliferative rather than degenerative condition[4,70] and UV light

427   alters cell proliferation at the limbal area as the first event promoting pterygium formation[78], an

428   MTT proliferation assay was then performed on HCE-S cells after UVA treatment (Fig.5B). UVA

429   significantly increased HCE-S proliferation at 72 hours (Δabsorbance at 72-24 hours, control

430   0.53 ± 0.02 OD vs UVA 0.6 ± 0.03 OD; p ≤ 0.05). When cells were transfected with 0.5nM

431   siCRIM1 prior to UVA treatment, HCE-S proliferation was further increased relative to UVA

432   treatment alone (Δabsorbance at 72-24 hours: 0.7 ± 0.02 OD, with p ≤ 0.05 compared to UVA

433   and p ≤ 0.01 compared to the mock NSC4 control).

434   As previously shown (Fig.4B), ERK phosphorylation was significantly increased 24 hours

435   after UV exposure. Transfection of cells with 0.5nM siCRIM1 prior to UV exposure almost

436   completely abolished the increase in ERK phosphorylation (Fig.5C).

437   Finally, ERK and *CRIM1* regulation were related to *BCL2* expression levels (Fig.5D), which

438   decreased significantly 24 hours after UVA treatment of HCE-S cells when compared with the

439   untreated control ($2^{-\Delta\Delta Ct}$ values for UVA treated HCE-S: 0.61 ± 0.06, p ≤ 0.01). However, prior

440   transfection with 0.5nM siCRIM1 prevented the decrease in *BCL2* expression, and was not

441   significantly different from mock NSC4 transfected cells ($2^{-\Delta\Delta Ct}$ values of siCRIM1+UVA: 0.96

442   ± 0.08).

443   The latest results obtained using siCRIM1 were able not only to confirm the previous data

444   showing a UVA-mediated increase in *CRIM1* expression, ERK phosphorylation and a decrease

445   in *BCL2* expression, but also to demonstrate that by modulating only *CRIM1* expression, the

446   whole signalling pathway leading to cell proliferation in response to UVA exposure can be

447   regulated.

448

449   *3.6 Effects of wild type and H412P mutant CRIM1 over-expression in HCE-S cells*

450   Based on the outlined pathway involving CRIM1 regulation upon UV exposed HCE-S cells, the

451   consequences of the H412P *CRIM1* variant in a pterygium pathogenic context were investigated.

452   The H412P variant was introduced into the human *CRIM1* sequence by site directed mutagenesis

453   and the complete *CRIM1* sequence checked by Sanger sequencing (Supplementary Table1),

454   confirming the presence of the c.1235 A>C substitution and absence of any other variation in the

455   sequence.

456   HCE-S cells were transfected with an empty plasmid, wild type or the *CRIM1*:p.H412P

457   expression plasmid. A significant *CRIM1* overexpression with respect to endogenous *CRIM1* was

458   revealed by qRT-PCR both at 48 hours (*CRIM1* wt 6 ± 0.82, $p<0.01$ and *CRIM1* H412P $5.8 \pm$

459   0.97, $p<0.05$) and at 72 hours (*CRIM1* wt 6.4 ± 1.075, $p<0.01$ and *CRIM1* H412P 6.3 ± 1.4

460    $p<0.01$) after transfection (Fig.6A).

461   Since a decrease in proliferation was reported in vascular endothelial cells after transient CRIM1

462   overexpression[54], an *in vitro* MTT proliferation assay was then performed in HCE-S cells

463   transfected with *CRIM1* wild type or H412P constructs (Fig.6B). Compared to mock transfected

464   HCE-S cells, wild type *CRIM1* overexpression had a relevant anti-proliferative effect, which was

465   most significant at 72 hours post-transfection (Δabsorbance 72-24 hours 0.60 ± 0.02 OD; $p<0.01$).

466   This effect was not observed in the *CRIM1* H412P transfected cells (Δabsorbance 72-24 hours

467   0.52 ± 0.02 OD), which did not differ significantly from the mock transfected control

468   (Δabsorbance 72-24 hours 0.57 ± 0.01 OD).

469   ERK phosphorylation is increased, simultaneously with CRIM1 expression, in vascular

470   endothelial cells after VEGFA treatment[79]. Here, ERK phosphorylation was strongly increased in

471   the wild type *CRIM1* transfected HCE-S compared to mock transfected control and to H412P

472   *CRIM1* transfected cells at 72 hours post-transfection (Fig.6C).

473   Other gene expression levels, possibly affected by *CRIM1* H412P variant, were investigated

474   by qRT-PCR: *VEGFA* for its role in pterygium angiogenesis[3,72] and its direct interaction with

475   *CRIM1*[73], Transforming Growth Factor beta I (*TGF-βI*) for its involvement in several other eye

476   diseases[80] and *BCL2* for its importance in apoptosis, previously documented in pterygium[77,81].

477   HCE-S cells were transfected with wild type and H412P *CRIM1* plasmids and gene expression

478   was assessed at 48 and 72 hours after transfection (Fig.6D). Levels of *VEGFA* and *TGF-βI*

479   expression were not significantly different between the wild type and the H412P *CRIM1*

480   transfected cells (*VEGFA*: wild type 48 hours 0.8351 ± 0.0740, H412P 48 hours 0.8966 ± 0.0630,

481   wild type 72 hours 1.1447 ± 0.0940, H412P 72 h 1.0443 ± 0.1100, *TGF-βI*: wild type 48h 0.7410

482   ± 0.0730, H412P 48h 0.8630 ± 0.0480, wild type 72h 0.9428 ± 0.0650, H412P 72h 1.1810 ±

483   0.1080, all values are expressed in $2^{-\Delta Ct}$). In contrast, a significant decrease in *BCL2* expression

484   level was observed in the wild type *CRIM1* transfected cells with respect to H412P mutant and

485   mock transfected cells (p value <0.05) both at 48 and 72 hours (wild type 48 hours: 0.5453 ±

486   0.0720, H412P 48 hours: 1.1647 ± 0.1800 and wild type 72 hours: 0.5977 ± 0.0240, H412P 72

487   hours: 1.2376 ± 0.1350, all values are expressed in $2^{-\Delta Ct}$), suggesting that overexpression of

488   *CRIM1* may play a role in up-regulation of apoptosis, which is normally induced in cornea and

489   conjunctiva by UV radiation[82,83].

490   The effect of increased *CRIM1* expression upon apoptosis in HCE-S cells was investigated in

491   *CRIM1* transfected cells by TUNEL assay (Fig.6E). At 72 hours after transfection the wild type

492   *CRIM1* transfected HCE-S cells showed a significantly higher rate of apoptosis compared to either

493   the H412P *CRIM1* or mock transfected HCE-S. The percentage of apoptotic (TUNEL positive),

494   wild type *CRIM1* transfected cells (25.6 ± 1.8) was significantly higher than either H412P *CRIM1*

495   plasmid or mock transfected HCE-S cells (3.9 ± 0.4 and 2.7 ± 0.5 respectively; p<0.001) (Fig.6E).

496   We have shown here that *CRIM1* plasmid overexpression exerts the same effects of UV induced

497   *CRIM1* increased intracellular levels, in terms of decreased cell proliferation, increase in ERK

498   phosphorylation and reduction in *BCL2* expression, followed by a higher rate of apoptosis.

499   The presence of H412P variant in *CRIM1* however abolished any of those effects, supporting a

500   role for this variant in the increased susceptibility of members of the Northern Irish family to

501   pterygium and pinguecula.

502

4. DISCUSSION

UV light presents a chronic stimulus to the eye surface, altering the normal processes of growth control in cornea and conjunctiva, and is associated with several pathologies affecting the anterior eye[84] such as photokeratitis[85], climatic droplet keratopathy[10], cortical cataract[86], squamous cell carcinoma[87] and pterygium[9,21]. Pterygium, resulting in 1% of all the ocular surgeries in developed countries[88] and presenting a 12% surgery recurrence rate[5], represents a substantial cost to National Health Services and the community, estimated in Australia as US \$100M per year[89]. In the identified Northern Irish family (Fig.1), affected by pterygium or pinguecula despite not being exposed to high levels of sunlight, genetic predisposition may play a fundamental role in the etiologic process (Table 1). A WES approach to candidate gene identification with *in silico* and literature analysis led to selection of H412P variant in *CRIM1* gene for several reasons. Firstly, the substitution of a highly conserved, positively charged histidine (H) residue with an apolar proline (P) is predicted to interfere with CRIM1 structure and function.

Moreover, the interaction between F1 domains of fibronectin, structurally similar to VWF domains of CRIM1 where H412P is located, and VEGF is enhanced at acidic pH (5.5-7)[66]. As Histidine works at this pH range ($pKa_3=6$), a mutation in this residue may interfere with the electrostatic binding of other ligands.

CRIM1's VWF domains (Fig.2) were also shown essential for interaction with VEGFA[62], the angiogenic factor overexpressed in the vascularised pterygium tissue following UV exposure[3,72]. CRIM1 is thus proposed as a VEGFA antagonist[60,73], possibly resisting pterygium formation by preventing angiogenesis as it has been shown to prevent proliferation[54,55]. Proliferation in cardiomyocytes is reduced by CRIM1 upregulation following miR199a silencing[55,56], the same miRNA which was found overexpressed in pterygium[90]. In addition to proliferation and angiogenesis, tissue remodelling through cell adhesion and migration also occurs during pterygium formation[4]. This process has been shown to be regulated by CRIM1 in neurons[57], lung

22

528   cancer[59] and lens epithelial cells[58], the latter showing a premature fibre differentiation when

529   *CRIM1* is lost[91].

530   As previously described, pterygium etiopathogenesis is generally ascribed to UV eye exposure

531   and *CRIM1* was found to be involved in UV related diseases such as bovine eye cancer[63] and

532   melanoma[64]. Finally, recent studies have elucidated the importance of *CRIM1* expression during

533   the anterior eye development[50,51,58].

534   *CRIM1* was thus selected as our best candidate responsible for pterygium pathogenesis within

535   the NI family. However, a reduced penetrance, as previously described in pterygium[1,26,31], makes

536   interpretation of genetic data challenging[36]. While two unaffected members of the NI family (III.2

537   and III.3) harbour the H412P variant in *CRIM*1, no affected member was found that did not have

538   the H412P variant. Moreover, given the younger age of the unaffected members (34 and 48 years

539   old), penetrance in this case could be age-related, as described in MEN1 syndrome, in which

540   tumour occurrence increases with the age, becoming fully penetrant only after sixty years[92]. It is

541   therefore possible that III.2 and III.3 family members may never develop pterygium or will do so

542   later in their lifetime; in any case, they should be monitored closely for development of pterygium

543   in the future.

544   Neither the *CRIM1* H412P variant nor any other alteration within the six VWFC domains of

545   *CRIM1* were found in other affected unrelated individuals from Northern Ireland.

546   Only one other patient from Bolivia was identified with a missense variant located between

547   VWFC-4 and VWFC-5: R745C (Supplementary Fig.1). While this arginine residue is not

548   conserved between the species, the introduction of a cysteine residue may facilitate disulphide

549   bridge formation with highly conserved cysteine residues in the previous or subsequent VWFC

550   domain, vital to the VWF domain's structure[45,93].

551   While no variants in *CRIM1* were found in the NI patients, CRIM1 expression was elevated

552   throughout the pterygium tissue compared to unaffected conjunctiva (Fig.3). In particular, *CRIM1*

553   expression was observed around pterygium blood vessels which, together with its previously

554 described expression in endothelial cells during capillary formation[60,61] and its interaction with

555 VEGFA[73], suggests a role for CRIM1 during the critical angiogenic processes of pterygium

556 formation[1,21]. CRIM1 was also detected in unusual structures such as hair follicles and sebaceous

557 glands, previously identified as characteristic features of some pterygia[70]. These structures are

558 representative of an uncontrolled transdifferentiation program[94] occurring in pterygium in

559 addition to an epithelial-mesenchymal transition (EMT) or fibrosis process[95], and likely reflects

560 similarities between pterygia, limbal dermoids and hair epithelia[96].

561 Comparing *CRIM1* expression levels between pterygium-affected and -unaffected individuals,

562 those were significantly increased in the affected samples (Fig.3G), while the lowest *CRIM1*

563 expression was recorded for the affected family member (II.2). A high *CRIM1* expression in

564 pterygium-affected individuals could therefore represent a defensive cellular response mechanism

565 against UV damaging effects, which is impaired by the H412P variant within the NI family.

566

567 Involvement of CRIM1 in UV-related diseases either in the eye[63] or the skin[64] is not surprising

568 considering that UV irradiation affects the balance between proliferation and apoptosis in several

569 cell types, including skin keratinocyes[97,98], corneal epithelium[82] and pterygium basal epithelial

570 cells[77]. However, while the eye is exposed to both UVA and UVB radiation, the intensity of UVA

571 radiation reaching the Earth's surface has 10-100 times the intensity of UVB[99] and it is known to

572 induce oxidative stress in exposed cells and tissues, including pterygium[100]. Accordingly, UVA

573 induced a more rapid and larger response than UVB in HCE-S cells (Fig.4A).

574 Exposure of HCE-S cells to UVA radiation leads to an increase in *CRIM1* (Fig.4A) expression.

575 The elevated ERK phosphorylation upon UVA irradiation we observed (Fig.4B) was previously

576 described in UVA or UVB irradiated pterygium and conjunctival cells[19,20]. While inhibition of

577 ERK phosphorylation alone had no effect on the expression of *CRIM1*, it potentiated the *CRIM1*

578 up-regulation when HCE-S cells were treated with UV (Fig.4C). This underscores the importance

579 of UV irradiation as the primary trigger for the intracellular pathway but underlines also the

24

580　　capacity of ERK phosphorylation to regulate *CRIM1* expression levels. Moreover, inhibition of

581　　ERK phosphorylation in HCE-S cells treated with UV abolished the UV-induced decrease in

582　　*BCL2* expression (Fig.4D): UV decreases *BCL2* levels through ERK phosphorylation, which

583　　results therefore in upstream *BCL2* regulation within this pathway.

584　　The role of CRIM1 in the cellular response to UV exposure was confirmed in HCE-S cells in

585　　which *CRIM1* over-expression induced by UV treatment was inhibited by siRNA transfection

586　　(Fig.5A). An increased cell proliferation in siCRIM1-treated cells upon UV exposure (Fig.5B),

587　　suggests that CRIM1 has a role in protecting against pterygium formation by minimising cell

588　　proliferation in response to UV radiation. When siCRIM1 was added to UV treatment, HCE-S

589　　cells decreased ERK phosphorylation to that seen in untreated cells (Fig.5C) and restored *BCL2*

590　　basal expression (Fig.5D), revealing that also *CRIM1* is able to control ERK phosphorylation as

591　　well as *BCL2* expression and locates it upstream of those two factors within the pathway. Those

592　　experiments showed how CRIM1 exerts a central role within the UV triggered intracellular

593　　pathway and silencing its expression is enough to counter all those alterations we examined.

594　　Previous studies have shown how *CRIM1* alterations influences cellular function: multiple exon

595　　deletions of *CRIM1* lead to syndromic disease[52] while a minor alternately spliced *Crim1* isoform

596　　determines perinatal lethality with multiple organ dysfunction[51]; however, the effects of *CRIM1*

597　　missense mutations still remain unexplored. Therefore, based on the intracellular mechanism

598　　described, the effects of the H412P variant found within the Northern Irish kindred were studied.

599　　*CRIM1* over-expression in HCE-S cells leads to reduced proliferation (Fig.6B) and a parallel

600　　increase in apoptosis (Fig.6D), as expected following the previous results where *CRIM1* was

601　　shown having a protective role in pterygium formation, counteracting the UV-induced

602　　proliferation (Fig.4B). This is in accordance with the downregulation of vascular endothelial cell

603　　proliferation after transient *CRIM1* overexpression[54] and with the increase in cardiomyocyte

604　　proliferation following *CRIM1* silencing through miR-199a[55,56]. Since the same miR-199a was

605　　found upregulated in pterygium[90], this could analogously increase cell proliferation in pterygium

606 formation through *CRIM1* silencing, counteracting the protective effects of *CRIM1*

607 overexpression.

608 *CRIM1* overexpression was also able to increase ERK phosphorylation (Fig.6B) following UVA

609 irradiation (Fig.4B). This result confirms previous data (Fig.5C) showing that the effects of

610 *CRIM1* overexpression lie upstream of ERK phosphorylation and demonstrates that it does not

611 need UV to exert its function.

612 All the effects of *CRIM1* overexpression in HCE-S cells were almost completely abolished by the

613 H412P variant in *CRIM1* (Fig.6).

614 The results obtained delineated a finely regulated pathway where either UV (Figure 4B) or

615 elevated CRIM1 levels (Figure 6C) increase ERK phosphorylation, demonstrating that CRIM1

616 lies upstream of, and is responsible for ERK phosphorylation.

617 CRIM1 expression was increased upon UV exposure and this increase was potentiated when the

618 U0126 inhibitor was added to the UV-irradiated cells. This suggests a feedback mechanism in

619 which ERK phosphorylation, increased by elevated *CRIM1* levels, serves to limit the rise in

620 *CRIM1* expression triggered by UV (Fig.7). UV is therefore necessary for the activation of the

621 whole pathway because the U0126 inhibitor alone, without UV treatment, does not increase

622 CRIM1 expression (Figure 4C). For the first time an increase in *CRIM1* expression has been

623 directly correlated with a consequent activation of the ERK pathway in corneal cells.

624 Based on the *in vitro* experimental evidence and on the feedback mechanism outlined, H412P can

625 be considered either a loss-of-function or a dominant-negative mutation. Similarly, a study on a

626 shortened mouse *Crim1* isoform was unable to conclude whether the mechanism was

627 hypomorphic (reduced activity) or dominant negative[51], although the latter have been described

628 in growth factor receptors which bind the same CRIM1 interactors such as PDGF[101] or VEGF[102]

629 and in VWF domains similar to those found in CRIM1[103,104].

630

631

632 **5. CONCLUSIONS**

633 In summary, we have shown that *CRIM1* plays an important role in the response of corneal

634 cells to UV irradiation by activation of a finely regulated intracellular pathway where increased

635 *CRIM1* expression counteracts cell proliferation and increases apoptosis. We demonstrate that

636 *CRIM1* H412P variant impairs this response, suggesting its involvement in the increased

637 susceptibility to pterygium observed in a Northern Irish family. Further investigation of the role

638 of CRIM1 in UV triggered pathways and pterygium holds promise as a target for the prevention

639 and treatment of development or recurrence of pterygium or other UV related diseases.

640

641

648

649

7.   FIGURE LEGENDS

A

B

C

Filters	No. of variants
WES	451,153
Ingenuity Confidence	30,000
Ingenuity Common Variants	25,000
Ingenuity Predicted Deleterious	11,000
Ingenuity Genetic Screening	40
In silico, literature	1

Figure 1. Northern Irish family affected by pterygium or pinguecula and WES analysis. **(A).** Pedigree of a Northern Irish family affected with pterygium. Open symbols denote unaffected individuals; filled black symbols denote pterygium affected individuals and filled black symbols with open circles inside denote pinguecula affected individuals. Squares represent male an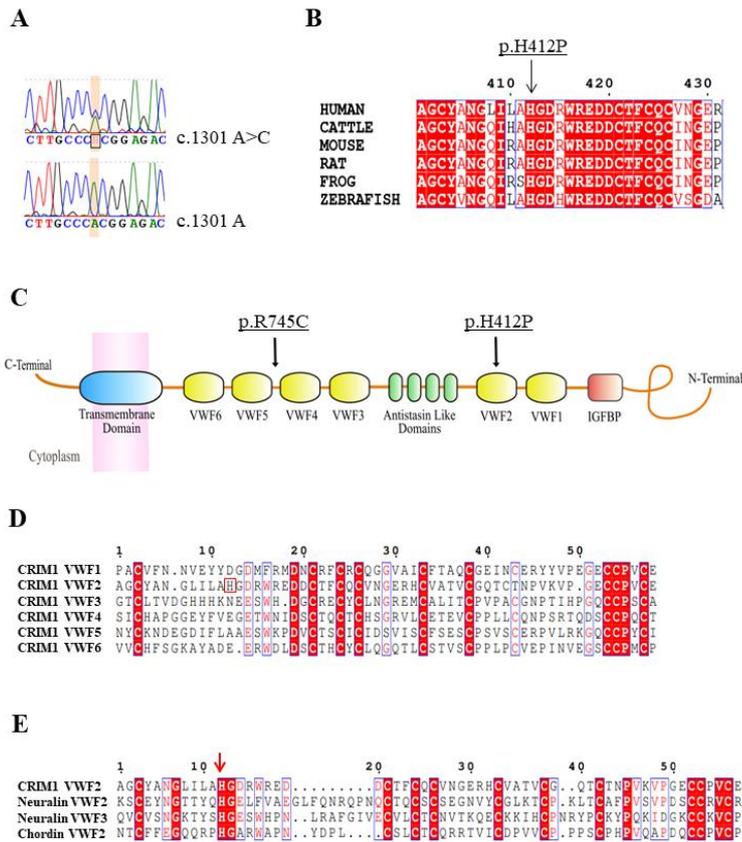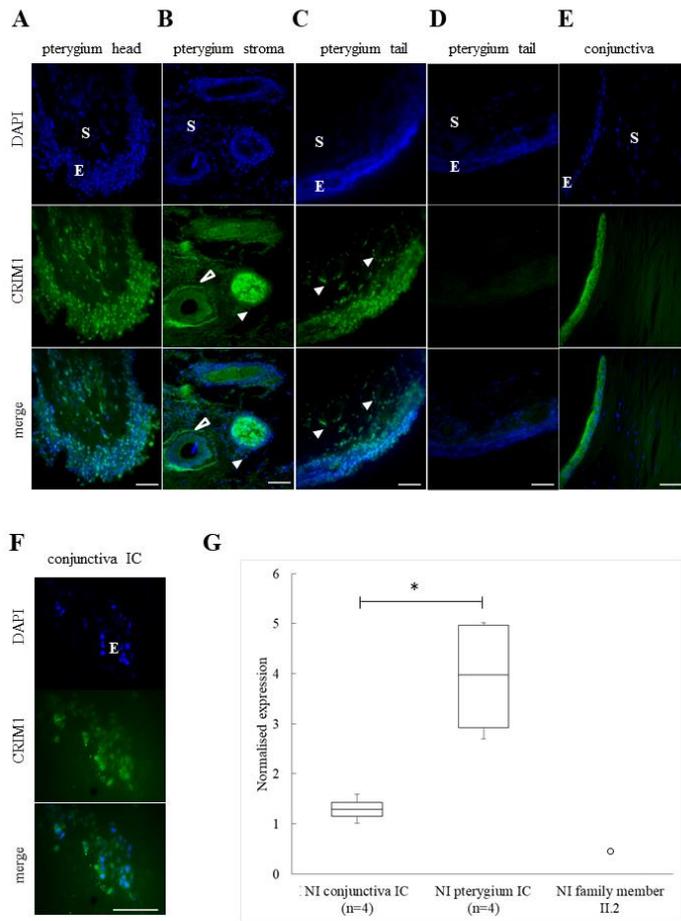d circles represent female individuals. Slashed symbols denote deceased family members and question marks are for individuals who have not participated in the study. Although all family members were invited to participate in this study, only those who gave informed consent were enrolled. **(B).** Pinguecula visible at the limbal area, between the cornea and conjunctiva (arrowhead). The image was obtained from family member III:5. **(C).** WES variants screening. Ingenuity variant analysis screened the 451,153 variants obtained with WES using four subsequent filters: Confidence to ensure quality, Common Variants (MAF < 0.05), Predicted deleterious using Polyphen and SIFT and Genetic, assuming an autosomal dominant inheritance pattern. A final *In silico* analysis based on the residue conservation through BLAST and Clustal Omega, expression analysis using TiGER database and literature research allowed selection of a single candidate variant in *CRIM1* gene.

Figure 2. CRIM1 (Cysteine RIch transMembrane BMP regulator 1) sequence in the NI family, conservation and structure analysis. **(A).** Electropherogram of Sanger sequencing performed in the family members confirmed the c.1235 A>C heterozygous transversion mutation in affected individuals and which was homozygous for wild-type A allele in the unaffected control. **(B).** Clustal X2.1 multiple sequence alignment of orthologous CRIM1 protein sequences from Human (NP_057525.1), Cattle (NP_001192227.1), Mouse (NP_056615.1), Rat (NP_001162574.1), Frog (NP_001163917.1), Zebrafish (NP_997986.1) indicates that the H412P missense mutation occurs in a highly conserved residue. EsPript 3.0. Legend: Red box, white character: strict identity; Red character: similarity in a group; Blue frame: Similarity **(C).** Schematic ideogram of Human CRIM1, characterised by multiple domains: one transmembrane (blue), six von Willebrand factor (VWF) (yellow), four antistasin-like (green) and one IGFBP (red). The position of the H412P and the R745C mutation are indicated. **(D).** Clustal X2.1 alignment of the six VWFC domains in *CRIM1* shows that, other than in VWFC-2, H412 is not conserved in the other five VWFC domains. **(E).** Clustal X2.1
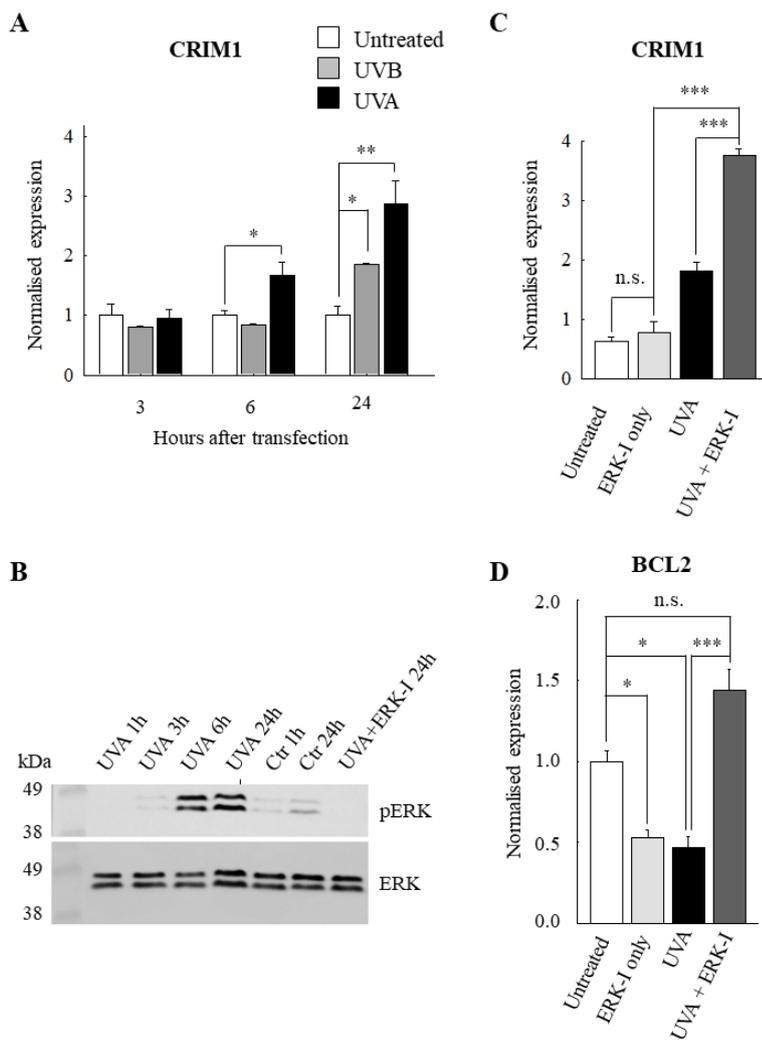
680   alignment of CRIM1 with other BMP antagonists indicates that the residue H412 is conserved in the

681   VWFC-2 domain of human chordin and in the VWFC-2 and 3 domains of human neuralin.

682   across groups (if more than 70% of the residues within the frame share similar physico-chemical

683   properties).

684

685

Figure 3. CRIM1 expression analysis in pterygium and conjunctiva from Northern Ireland. **A-F** images represent immunohistochemical (IHC) staining of CRIM1 expression (green) and nuclei (DAPI, blue) in pterygium and conjunctival tissues obtained from sporadic Northern Irish patients. Scale bar, 100μm **(A).** CRIM1 expression in a pterygium head, visible in both the external epithelial layer (E) as well as the internal stroma (S). **(B)**. CRIM1 expression shown in peculiar structures identified in pterygium stroma: a hair follicle (empty arrowhead) and a sebaceous gland (plain arrowhead). **(C).** CRIM1 expression in pterygium tail, arrowheads indicate CRIM1 expression in cells surrounding the blood vessels. **(D).** Negative IgG control in pterygium tail tissue. **(E).** CRIM1 expression in conjunctival epithelial tissue of an unaffected individual. **(F).** IHC of a post-surgical impression cytology sample obtained from unaffected superficial epithelial conjunctival cells: CRIM1 is expressed in all the cells captured on the membrane filter. **(G)** *CRIM1* expression is

31

697 increased in pterygium patients from Northern Ireland. qRT-PCR analysis of *CRIM1* carried out in

698 cDNA from post-surgical impression cytology samples: NI conjunctival individual controls, NI

699 pterygium individuals and one affected NI family member (II.2 in Fig. 1). All values are expressed

700 in $2^{-\Delta Ct} \pm$ SEM. n=2 with two technical replicates each sample.

701

Figure 4. UV treatment of HCE-S cells increases CRIM1 expression, ERK phosphorylation and decreases BCL2 expression. **(A).** qRT-PCR revealed significantly increased CRIM1 expression levels in HCE-S cells at 6 ($p \leq 0.05$) and 24 hours ($p \leq 0.01$) after UVA treatment and at 24 hours ($p \leq 0.05$) after UVB treatment compared to the untreated control. **(B).** Western blot analysis of HCE-S cell lysates revealed an increase in ERK phosphorylation at 6 and 24 hours after UVA irradiation with respect to ERK phosphorylation levels of untreated control. Pretreatment of cells with U0126 inhibitor abolished ERK phosphorylation in UV treated cells. **(C).** qRT-PCR was used to evaluate *CRIM1* expression following UV treatment in the presence of MEK1/2 inhibitor, U0126. Inhibition of ERK pathway activation enhances the increase in *CRIM1* expression seen in UV irradiated HCE-S cells whilst inhibition of ERK phosphorylation alone has no significant effect. **(D).** *BCL2* expression measured by qRT-PCR. HCE-S cells were UVA irradiated with and without U0126 and

33

714   harvested 24 hours after treatment. A significant decrease in *BCL2* expression was observed when

715   the cells were treated with either U0126 or UVA alone but not in combination when compared to the

716   HCE-S untreated cells. qRT-PCR data represent fold change of the $2^{-\Delta\Delta Ct}$ mean $\pm$ SEM compared to

717   untreated HCE-S. n=3 with three technical replicates each.

718

Figure 5. siCRIM1 0.5nM is able to restore normal HCE-S conditions after UVA treatment. **(A).**

qRT-PCR shows the amount of siCRIM1 (0.5nM) able to restore endogenous CRIM1 levels in

HCE-S after UVA exposure. For all the experiments HCE-S cells were treated with: NSC4, UVA +

NSC4 and UVA+ siCRIM1 (0.5nM) and harvested 24 hours later. Data represent $2^{-\Delta Ct} \pm$ SEM. n=3

with three technical replicates for each sample. **(B).** An MTT assay demonstrates an increased

proliferation upon UVA exposure, which is further increased if *CRIM1* expression is restored to

pre-treatment endogenous levels (siRNA 0.5nM), confirming the antiproliferative effect of CRIM1.

n=6 with eight technical replicates for each condition. **(C).** Western Blot analysis shows ERK

phosphorylation (pERK) at 24 hours after UVA treatment in HCE-S cells. The increased ERK

phosphorylation due to UVA exposure was brought back to normal levels following transfection

with 0.5nM CRIM1 siRNA. **(D).** *BCL2* expression, measured by qRT-PCR, decreases upon UVA

731   irradiation eliciting apoptosis but is restored in HCE-S cells treated with siCRIM1. Data represent 2^-

732    $^{\Delta\Delta Ct} \pm$ SEM with respect to untransfected HCE-S. n=3 with three technical replicates each sample.

733

734

Figure 6. *CRIM1* wild type overexpression in HCE-S cells results in a decrease in cell proliferation and an increase in ERK phosphorylation and apoptosis. **(A).** qRT-PCR showing *CRIM1* overexpression in mRNA obtained from HCE-S cells transfected with Human *CRIM1* wild type and mutant (H412P) in pcDNA3.1 expression plasmid. Both *CRIM1* wild type (wt) and H412P mutant were significantly overexpressed at 48 and 72 hours after transfection with respect to the mock control. Data represent fold change of the $2^{-\Delta Ct}$ mean ± SEM. n=3 with 3 technical replicates for each condition. **(B).** An MTT assay of HCE-S cell proliferation was performed at 72 hours after transfection with empty plasmid (mock), *CRIM1* wt and H412P mutant constructs. *CRIM1* wt, when overexpressed, has an anti-proliferative effect when compared to the mock transfected control (p<0.001). Overexpression of the mutated H412P *CRIM1* does not have the same anti-proliferative

745　effect. n=6 with 8 technical replicates for each condition. **(C).** ERK phosphorylation (pERK) was

746　detected by Western Blot analysis at 72 hours post transfection with mock, *CRIM1* wt and H412P

747　plasmids in HCE-S cells. *CRIM1* wt overexpression resulted in a high level of ERK phosphorylation

748　in comparison to *CRIM1* H412P and mock control. **(D).** qRT-PCR analysis of *VEGFA*, *TGF-βI* and

749　*BCL2* expression in HCE-S cells transfected with mock, CRIM1 wt and H412P plasmids and

750　harvested after 48 and 72 hours. No significant variation of *VEGFA* and *TGF-βI* expression was

751　observed between mock, *CRIM1* wt and *CRIM1* H412P while *BCL2* expression significantly

752　decreased in H412 wt CRIM1 transfected cells compared with mock transfected HCE-S both at 48

753　and 72 hours post transfection. Data represent fold change of the $2^{-\Delta Ct}$ mean ± SEM respect to mock

754　transfected HCE-S. n=3 with three technical replicates each. **(E).** TUNEL assay in HCE-S cells

755　transfected with wt and H412P mutant *CRIM1* plasmids. TUNEL-positive cells are stained green and

756　nuclei are stained blue with DAPI. Overexpression of CRIM1 wt results in increased apoptosis

757　compared to either the *CRIM1* H412P or mock transfected cells. Scale bar, 100 μm. TUNEL assay

758　quantification was performed in 12 fields per condition using ImageJ. n=3

759

760

761

762

763

Figure 7. CRIM1 regulates pERK in a looped pathway. Here, based on our experimental evidence,

we propose, within a schematic, an intracellular pathway triggered by UV that may act as a

protective mechanism against pterygium development. When cells are exposed to UV light, CRIM1

expression is increased, which in turn increases ERK phosphorylation. This, in turn, blocks further

CRIM1 expression in the feedback loop shown. Inhibition of ERK phosphorylation prevents this

negative feedback, resulting in further increases of CRIM1 expression.

ERK phosphorylation induces decreased expression of the anti-apoptotic BCL2, initiating cell

apoptosis. This proposed pathway was shown to be impaired in the case of the H412P mutation in

CRIM1, found in the Northern Irish family affected by pterygium.

773

774

39

775

Supplementary Figure 1. R745C variant found in a pterygium affected patient from Bolivia. **(A).**
Electropherogram showing the novel c.2299C>T transition variant from the Bolivian patient (B1),
which corresponds to the R745C variant**. (B).** Multiple *CRIM1* sequence alignment shows that the
R745 residue is not conserved across species; it is conserved however the absence of cysteine between
VWFC-4 (residues 677-735) and VWFC-5 (residues 751-809).

781

Supplementary Figure 2. siRNAs targeting *CRIM1* efficiently knock down its expression in HCE-
S cells. *CRIM1* expression obtained using qRT-PCR of HCE-S cell cDNA 48 hours post transfection.
All four siRNAs tested were able to knock down *CRIM1* expression, including the pool of four
siRNAs used at the same final concentration of 10 nM. qRT-PCR data represent fold change of the
$2^{-\Delta\Delta Ct}$ mean $\pm$ SEM with respect to untreated HCE-S. n=2 with three technical replicates each.

787

CRIM1

788

Supplementary Figure 3. A dose response curve shows that 0.5nM siRNA pool restores HCE-S
endogenous *CRIM1* levels. *CRIM1* expression obtained using qRT-PCR of HCE-S cell cDNA 48
hours post transfection with UVA and the siRNA pool at different concentrations. qRT-PCR data
represent fold change of the $2^{-\Delta\Delta Ct}$ mean $\pm$ SEM with respect to untreated HCE-S. n=2 with three
technical replicates each.

794

TABLES

Family member	Year of birth	Sex	Eye condition	Age of diagnosis	Lived abroad	Time in sunny climates	Wear sunglasses
II.2	1944	F	pterygium	40 years	No	1/year, 3 weeks	Sometimes
II.4	1946	F	pterygium	59 years	Canada 13 years	1/year, 2 weeks	No
II.9	1958	M	unaffected	-	No	1/year, 3 weeks	Yes
II.14	1951	M	pterygium	62 years	No	1/year, 1 week	Yes
III.2	1967	M	unaffected	-	No	1/year, 1 week	Yes
III.3	1982	F	unaffected	-	No	1/year, 1 week	Sometimes
III.5	1968	F	pinguecula	38 years	Canada 13 years	1/year, 2 weeks	Sometimes
III.6	1970	F	pinguecula	40 years	Canada 13 years	1/year, 2 weeks	Sometimes

796

797   **Table 1.** Questionnaire results. The Northern Irish family members participating in the study are

798   listed with age of pterygium diagnosis, averaged 48 years old. The family were shown not to have

799   had excessive exposure to the sun, spending time in sunny climates from 1 to 3 weeks per years with

800   most stating that they wear sunglasses.

801

Gene Symbol	Chr	Position	Gene Region	Protein Variant	Conservation to:	Gene expressed in:	Associated Diseases
CTRC	1	15764869	Promoter		Human	pancreas, liver, spleen	chronic pancreatitis
KIF21B	1	200978030	Exonic	p.T105M	Elephant	eye (cornea), brain, blood	multiple sclerosis, inflammatory bowel disease
GALNT14	2	31348076	Intronic; Exonic; 5'UTR	p.A58V	Human	kidney, PNS, blood, eye	breast cancer
CRIM1	2	36706700	Exonic	p.H412P	Lamprey	placenta, kidney, PNS, eye	syndactyly, neuronitis, bovine ocular carcinoma
SPTBN1	2	54886366	Exonic	p.T2107A; p.T2094A	Dog	tongue, soft tissue, eye	fissured tongue, and buphthalmos
VRK2	2	58313555	Exonic; ncRNA	p.G113E; p.G90E	Elephant	lymph node, testis, colon	vaccinia, and hypoxia
PLEK	2	68615546	Exonic	p.N229H	X_tropicalis	bone marrow, lymph node, eye	aarskog-scott syndrome, centronuclear myopathy
HNMT	2	138772049	3'UTR		Dog	bladder, kidney, liver, eye	asthma, eosinophilia-myalgia syndrome
ITGB6	2	160994200	Exonic	p.H469N	Mouse	pancreas, tongue, stomach, eye	bullous keratopathy, mouth disease
WDR12	2	203760891	Exonic	p.L169S	Zebrafish	blood, intestine, thymus, eye	gigantism, and neuronal ceroid lipofuscinosis
CLDN16	3	190106072	Exonic	p.A56fs*16	Rhesus	kidney, ovary, uterus	nephrocalcinosis, and hypomagnesemia primary
CLDN16	3	190106074	Exonic	p.A56P	Rhesus	kidney, ovary, uterus	nephrocalcinosis, and hypomagnesemia primary
PRIM2	6	57398226	Exonic	p.G310V	Human	thymus, ovary, mammary, eye	
STK31	7	23811795	Exonic; ncRNA	p.N598_S600delinsKKI	Elephant	testis	
TYW1	7	66660242	Exonic	p.H632R	Human	stomach, heart, colon, eye	fanconi's anemia, and cytochrome p450
GLDC	9	6556206	Exonic	p.I717V	Zebrafish	small intestine, kidney, liver, eye	glycine encephalopathy
IFNA5	9	21304891	Exonic	p.C122S	Elephant	_____	hemorrhagic fever
DMRTA1	9	22451120	Exonic	p.K242R	Rhesus	_____	metabolic acidosis, prostatitis
MIR4289	9	91360776	microRNA		Dog	_____	
HBG2	11	5276282	Promoter		Rhesus	spleen, thymus, liver	sulfhemoglobinemia, cavernous hemangioma
OR4C16	11	55339462	Promoter		Human	_____	neuronitis
OR10AG1	11	55735808	Exonic	p.H43D	Rhesus	_____	neuronitis
C12orf56	12	64712620	Exonic; Intronic	p.T210I	Human	_____	
ATP8B4	15	50223420	Exonic; ncRNA	p.R513Q	Lamprey	blood, bone marrow	intrahepatic cholestasis
DMXL2	15	51773329	Exonic	p.D1356N; p.D1992N	Chicken	blood, testis, heart, eye	gynecomastia, and myocardial infarction
TPSD1	16	1306802	Exonic	p.I87V	Human	_____	asthma, allergic and inflammatory disorders
TPSD1	16	1306817	Exonic	p.A92T	Human	_____	asthma, allergic and inflammatory disorders
NOMO1	16	18544469	Exonic	p.R418H	Chicken	intestine, cervix, colon, eye	pseudoxanthoma elasticum (PXE)
SRCAP	16	30731568	Exonic	p.R968H	Chicken	Larynx, thymus, spleen, eye (cornea)	floating-harbor syndrome, Eosinophilic angiocentric fibrosis
ZNF319	16	58031913	Exonic	p.A86V	Elephant	bladder, blood, tongue	
PDPR	16	70154480	Exonic	p.T29A	Human	heart, bone, Eye	sarcosinemia
ZFHX3	16	72832474	Exonic	p.454_455insH; p.1368_1369insH	X_tropicalis	_____	prostate cancer, acute myocardial infarction
WWOX	16	78466409	Exonic	p.L272F	Rhesus	mammary, tongue, PNS, eye	toxic pneumonitis, andaspiration pneumonitis
GSDMA	17	38122680	Exonic	p.V128L	Human	_____	atopy, gastric cancer
DNAI2	17	72306188	Intronic; Exonic	p.V460V	Elephant	testis, uterus, lung, brain	ciliary dyskinesia
MAN2B1	19	12774537	Exonic	p.P248L	Dog	bone, PNS, intestine, eye	alpha-mannosidosis, alpha-mannosidosis, adult form
CYP4F2	19	15989730	Exonic	p.T472A	Mouse	intestine, blood, liver, muscle	warfarin sensitivity, cytochrome p450
PRKD2	19	47204207	Exonic	p.V167M; p.V324M	Lamprey	Spleen, tongue, ovary, eye	polycystic kidney disease, gastric cancer
NLRP7	19	55451405	Exonic	p.P261Q	X_tropicalis	_____	gestational trophoblastic neoplasm, hydatidiform mole
TTC3	21	38569884	Exonic	p.G1865S	X_tropicalis	Tongue, uterus, heart, eye	down syndrome critical region, down syndrome

Gene Symbol	Translation Impact	SIFT Function Prediction	SIFT Score	PolyPhen-2 Function Prediction	dbSNP ID	NHLBI ESP European Frequency (%)	Co-segregation within the family (IGV)					
							II.2	II.4	III.5	III.6	II.14	II.9
CTRC					144717165		Het	Het	Hom WT	Het	Het	Hom WT
KIF21B	missense	Damaging	0,01	Benign	150551633	0,01	Het	Het	Het	Het	Het	Hom WT
GALNT14	missense	Tolerated	0,26	Benign	41280621		Het	Het	Het	Het	Het	Hom WT
CRIM1	missense	Damaging	0,01	Probably Damaging	113372122	0,29	Het	Het	Het	Het	Het	Hom WT
SPTBN1	missense	Tolerated	0,72	Benign	147989241	0,16	Het	Het	Het	Hom WT	Het	Hom WT
VRK2	missense	Damaging	0,02	Benign	147530902	0,36	Het	Het	Het	Hom WT	Het	Hom WT
PLEK	missense	Tolerated	0,52	Benign	34338164	1,14	Het	Het	Het	Hom WT	Het	Hom WT
HNMT							Het	Het	Het	Hom WT	Het	Hom WT
ITGB6	missense	Tolerated	0,65	Benign	142197545	0,29	Het	Het	Hom WT	Het	Het	Hom WT
WDR12	missense	Damaging	0	Possibly Damaging		0	Het	Het	Hom WT	Het	Het	Hom WT
CLDN16	frameshift				56086318	0	Het	Het	Het	Het	Het	Hom WT
CLDN16	missense	Damaging	0,04	Benign	3214506	0	Het	Het	Het	Het	Het	Hom WT
PRIM2	missense				77436138		Het	Het	Het	Het	Het	Hom WT
STK31	in-frame					0	Het	Het	Het	Het	Het	Hom WT
TYW1	in-frame	Tolerated	0,5	Benign		0	Het	Het	Het	Het	Het	Hom WT
GLDC	missense	Tolerated	1	Benign	117460214	0,03	Het	Het	Hom WT	Het	Het	Hom WT
IFNA5	missense	Damaging	0	Probably Damaging	140371188	0,59	Het	Het	Hom WT	Hom WT	Het	Hom WT
DMRTA1	missense	Tolerated	0,54	Benign	145718826	0,38	Het	Het	Hom WT	Hom WT	Het	Hom WT
MIR4289							Het	Het	Het	Hom WT	Het	Hom WT
HBG2					113622787		Het	Het	Het	Hom WT	Het	Hom WT
OR4C16							Het	Het	Hom m	Het	Het	Hom WT
OR10AG1	in-frame	Activating	1	Benign		0	Het	Het	Hom m	Het	Het	Hom WT
C12orf56	missense	Tolerated	0,13		367932023	0,03	Het	Het	Hom WT	Het	Het	Hom WT
ATP8B4	missense	Damaging	0	Probably Damaging		0	Het	Het	Hom WT	Het	Het	Hom WT
DMXL2	missense	Tolerated	0,17	Benign	144241909	0,02	Het	Het	Hom WT	Het	Het	Hom WT
TPSD1	missense	Tolerated	0,31	Benign	2401930	0	Het	Het	Het	Het	Het	0
TPSD1	missense	Tolerated	0,75	Benign	3993983	0	Het	Het	Het	Het	Het	0
NOMO1	missense	Tolerated	0,23	Benign	140359200	0,12	Het	Het	Hom WT	Hom WT	Het	Hom WT
SRCAP	missense	Damaging	0	Possibly Damaging	368876335	0,01	Het	Het	Hom WT	Het	Het	Hom WT
ZNF319	missense	Tolerated	0,08	Benign		0	Het	Het	Hom WT	Het	Het	0
PDPR	missense	Tolerated	1	Benign	200469748	0	Het	Het	Het	Het	Het	Het
ZFHX3	in-frame					0	Het	Het	Hom WT	Het	Het	Hom WT
WWOX	missense	Tolerated	0,7	Benign	186745328	0,46	Het	Het	Hom WT	Het	Het	Hom WT
GSDMA	missense	Activating	1	Benign		0	Het	Het	Het	Het	Het	Hom WT
DNAI2	synonymous				148947094	0,05	Het	Het	Hom WT	Het	Het	Hom WT
MAN2B1	missense	Damaging	0,01	Possibly Damaging	117843968	0,42	Het	Het	Het	Het	Het	Hom WT
CYP4F2	missense	Tolerated	0,39	Benign	4020346	0	Het	Het	Hom WT	Hom WT	Het	Hom WT
PRKD2	missense	Tolerated	0,15	Benign	45455991	0,98	Het	Het	Hom WT	Het	Het	Hom WT
NLRP7	missense	Damaging	0	Probably Damaging		0	Het	Het	Het	Hom WT	Het	Hom WT
TTC3	missense	Tolerated	0,55	Possibly Damaging		0	Het	Het	Het	Hom WT	Het	Hom WT

803

804 **Table 2.** Candidate genes analysis. The table shows the 40 genes obtained from Ingenuity and the

805 analysis done for each of the associated variants. The selection was mainly based on the expression

806 of the gene in the eye (TIGER database), the SIFT and Polyphen predictions and known diseases

807 association (literature review). Subsequently the aminoacid conservation through vertebrate species

808 (BLAST analysis) and co-segregation of the mutation in pterygium (II.2, II.4, II.14) and pinguecula

809 (III.5, III.6) affected members and not in the II.9 unaffected family member (IGV analysis) was

810 considered. This screening led to the selection of *CRIM1* as the best candidate considering those

811 parameters.

812

813 A.

Patient NI	Year of birth	Sex	Eye condition
1	1942	M	pterygium
2	1950	M	minor pterygium
3	1931	M	pterygium
4	1954	M	pterygium
5	1946	M	pterygium
6	1975	M	pterygium
7	1941	M	pterygium
8	1958	F	pterygium
9	1984	F	pterygium
10	1934	M	pterygium
11	1974	F	pterygium
12*	1967	F	pterygium family

814

815

816

817

818   B.

Patient Bolivia	Year of birth	Sex	Eye condition
B1	1965	F	pterygium
B2		M	pterygium
B3	1949	M	pterygium
B4	1957	M	pterygium
B5	1999	M	pterygium
B6	1952	M	pterygium
B7	1947	F	pterygium
B8	1941	M	pterygium
B9	1990	M	pterygium

819

820 **Table 3.** Individual pterygium participants. **(A).** A list of pterygium affected individuals collected in

821 the UK and the relevant information obtained through the questionnaire. *Patient 12 denotes the

822 pterygium affected II.1 family member previously studied[27]. **(B).** List of pterygium affected

823 individuals collected in Bolivia and the year of birth and sex of participants.

824

825

826

827

828

829

830

831

832

833

CRIM1 sequence	Primer sequence (5' to 3')
T7_F	TAATACGACTCACTATAGGG
Seq1_R	GCAGAATGTGCAGTCGTCTT
Seq1_F	TGATCGAGGGTTATGCTCCT
Seq2_F	TACTACGTGCCCGAAGGAGA
Seq2_R	GGCACTTTCACAGGGTTTGT
Seq3_F	TGCCGGGAATGCTACTGT
Seq3_R	ACAGAAGGGCAGGACTCAGA
Seq4_F	CTGAGTCCTGGAAGCCTGAC
Seq4_R	CCTGGAGGTGACCCATATCT
Seq5_F	AACCATCGAGGAGAGGTTGA
Seq5_R	TCGTCTTCCGTCTTTTGAAAC

834

835 **Supplementary Table 1.** Primers used to validate that the whole of the CRIM1 sequence was inserted

836 into the pcDNA3.1 plasmid and to check the presence of the H412P mutation introduced by site

837 directed mutagenesis.

838

839

CRIM1 VWFs	Primer sequence (5' to 3')
Exon6_F (VWF1)	TTGAAAAACATCAAAGGACACAA
Exon6_R (VWF1)	CCATGTATGCTCCTGTTAATCTG
Exon7_F (VWF2)	GATGACTAGAACCCAGGGAAAA
Exon7_R (VWF2)	AGCAGACATTATGCCCAAGG
Exon11_F (VWF3)	GCCTGTTTCTCCTGTGCAGT
Exon11_R (VWF3)	TGCAAGGCAGAAGTCATTTG
Exon12_F (VWF4)	CCAGGCTTTCAAGAGTTGGA
Exon12_R (VWF4)	GGGTCCCACAGAATGACAAC
Exon13_F (VWF5)	CTGGCCAACAGCATCTTCTT
Exon13_R (VWF5)	GACATGTCAAGCAGGGAAAAA
Exon14_F (VWF6)	AAGATCGTGTGCGTTGTCAC
Exon14_R (VWF6)	GTCGAGCTCTGCTTCGATTT

840

841 **Supplementary Table 2.** Primers used to verify the presence of other mutations in all the VWF

842 domains of CRIM1.

843

8. REFERENCES

1   Chui, J., Di Girolamo, N., Wakefield, D. & Coroneo, M. T. The pathogenesis of pterygium: current concepts and their therapeutic implications. *The ocular surface* **6**, 24-43 (2008).

2   Das, P. *et al.* Limbal epithelial stem-microenvironmental alteration leads to pterygium development. *Molecular and cellular biochemistry* **402**, 123-139, doi:10.1007/s11010-014-2320-z (2015).

3   Bianchi, E. *et al.* Immunohistochemical profile of VEGF, TGF-beta and PGE(2) in human pterygium and normal conjunctiva: experimental study and review of the literature. *Int J Immunopathol Pharmacol* **25**, 607-615 (2012).

4   Detorakis, E. T. & Spandidos, D. A. Pathogenetic mechanisms and treatment options for ophthalmic pterygium: trends and perspectives (Review). *International journal of molecular medicine* **23**, 439 (2009).

5   Ono, T. *et al.* Long-term follow-up of transplantation of preserved limbal allograft and amniotic membrane for recurrent pterygium. *Graefe's Archive for Clinical and Experimental Ophthalmology*, 1-6 (2016).

6   Kaji, Y. *et al.* Immunohistochemical localization of advanced glycation end products in pinguecula. *Graefe's archive for clinical and experimental ophthalmology = Albrecht von Graefes Archiv fur klinische und experimentelle Ophthalmologie* **244**, 104-108, doi:10.1007/s00417-005-0047-y (2006).

7   Jakobiec, F. A., Rashid, A., Bozorg, M. S. & Dana, R. Unusual large uniocular elastoid and collagenous pinguecula. *Graefe's archive for clinical and experimental ophthalmology = Albrecht von Graefes Archiv fur klinische und experimentelle Ophthalmologie* **252**, 1173-1175, doi:10.1007/s00417-014-2649-8 (2014).

8   Lemercier, G., Cornand, G. & Burckhart, M. F. [Pinguecula and pterygium: histologic and electron microscopic study (author's transl)]. *Virchows Archiv. A, Pathological anatomy and histology* **379**, 321-333 (1978).

9   Moran, D. J. & Hollows, F. C. Pterygium and ultraviolet radiation: a positive correlation. *British Journal of Ophthalmology* **68**, 343-346 (1984).

10   Taylor, H. R. *et al.* Corneal changes associated with chronic UV irradiation. *Archives of Ophthalmology* **107**, 1481-1484 (1989).

11   McCarty, C. A., Fu, C. L. & Taylor, H. R. Epidemiology of pterygium in Victoria, Australia. *British Journal of Ophthalmology* **84**, 289-292 (2000).

12   Zhong, H. *et al.* Ethnic Variations in Pterygium in a Rural Population in Southwestern China: The Yunnan Minority Eye Studies. *Ophthalmic Epidemiol* **23**, 116-121, doi:10.3109/09286586.2015.1099685 (2016).

13   Gazzard, G. *et al.* Pterygium in Indonesia: prevalence, severity and risk factors. *British journal of ophthalmology* **86**, 1341-1346 (2002).

14   Lombardo, M., Pucci, G., Barberi, R. & Lombardo, G. Interaction of ultraviolet light with the cornea: clinical implications for corneal crosslinking. *Journal of cataract and refractive surgery* **41**, 446-459, doi:10.1016/j.jcrs.2014.12.013 (2015).

15   Coroneo, M., Müller-Stolzenburg, N. & Ho, A. Peripheral light focusing by the anterior eye and the ophthalmohelioses. *Ophthalmic Surgery, Lasers and Imaging Retina* **22**, 705-711 (1991).

16   Kau, H. C., Tsai, C. C., Hsu, W. M., Liu, J. H. & Wei, Y. H. Genetic polymorphism of hOGG1 and risk of pterygium in Chinese. *Eye (Lond)* **18**, 635-639, doi:10.1038/sj.eye.6700738 (2004).

17   Tsai, Y. Y. *et al.* Null type of glutathione S-transferase M1 polymorphism is associated with early onset pterygium. *Mol Vis* **10**, 458-461 (2004).

18   Di Girolamo, N., Wakefield, D. & Coroneo, M. T. UVB-mediated induction of cytokines and growth factors in pterygium epithelial cells involves cell surface receptors and

844
845
846
847
848
849
850
851
852
853
854
855
856
857
858
859
860
861
862
863
864
865
866
867
868
869
870
871
872
873
874
875
876
877
878
879
880
881
882
883
884
885
886
887
888
889
890
891
892
893

894		intracellular signaling. *Invest Ophthalmol Vis Sci* **47**, 2430-2437, doi:10.1167/iovs.05-1130
895		(2006).
896	19	Di Girolamo, N., Coroneo, M. T. & Wakefield, D. UVB-elicited induction of MMP-1
897		expression in human ocular surface epithelial cells is mediated through the ERK1/2 MAPK-
898		dependent pathway. *Investigative ophthalmology & visual science* **44**, 4705-4714 (2003).
899	20	Chao, S. C. *et al.* Ultraviolet-A irradiation upregulated urokinase-type plasminogen activator
900		in pterygium fibroblasts through ERK and JNK pathways. *Invest Ophthalmol Vis Sci* **54**,
901		999-1007, doi:10.1167/iovs.12-10469 (2013).
902	21	Coroneo, M. T. Pterygium as an early indicator of ultraviolet insolation: a hypothesis. *The*
903		*British journal of ophthalmology* **77**, 734-739 (1993).
904	22	Gallagher, M. J., Giannoudis, A., Herrington, C. S. & Hiscott, P. Human papillomavirus in
905		pterygium. *The British journal of ophthalmology* **85**, 782-784 (2001).
906	23	Piras, F. *et al.* Detection of human papillomavirus DNA in pterygia from different
907		geographical regions. *The British journal of ophthalmology* **87**, 864-866 (2003).
908	24	BOOTH, F. Heredity in one hundred patients admitted for excision of pterygia. *Australian*
909		*and New Zealand journal of ophthalmology* **13**, 59-61 (1985).
910	25	Ang, M. *et al.* Prevalence of and racial differences in pterygium: a multiethnic population
911		study in Asians. *Ophthalmology* **119**, 1509-1515 (2012).
912	26	Zhang, J. D. An investigation of aetiology and heredity of pterygium. Report of 11 cases in a
913		family. *Acta Ophthalmol (Copenh)* **65**, 413-416 (1987).
914	27	Romano, V., Steger, B., Kovacova, A., Kaye, S. B. & Willoughby, C. E. Further evidence
915		for heredity of pterygium. *Ophthalmic genetics*, 1-3, doi:10.3109/13816810.2015.1111911
916		(2016).
917	28	Hecht, F. & Shoptaugh, M. G. Winglets of the eye: dominant transmission of early adult
918		pterygium of the conjunctiva. *J Med Genet* **27**, 392-394 (1990).
919	29	Contrucci Faraldi, N. & Gracis, G. Pterygium on twins. *Ophthalmologica* **172**, 361-366
920		(1976).
921	30	Hill, J. C. & Maske, R. Pathogenesis of pterygium. *Eye (Lond)* **3 (Pt 2)**, 218-226,
922		doi:10.1038/eye.1989.31 (1989).
923	31	Islam, S. I. & Wagoner, M. D. Pterygium in young members of one family. *Cornea* **20**, 708-
924		710 (2001).
925	32	Tsai, Y.-Y. *et al.* Null type of glutathione S-transferase M1 polymorphism is associated with
926		early onset pterygium. *Molecular vision* **10**, 458-461 (2004).
927	33	Tsai, Y. Y. *et al.* Pterygium and genetic polymorphism of DNA double strand break repair
928		gene Ku70. *Mol Vis* **13**, 1436-1440 (2007).
929	34	Demurtas, P. *et al.* Association between the ACE insertion/deletion polymorphism and
930		pterygium in Sardinian patients: a population based case-control study. *BMJ open* **4**,
931		e005627, doi:10.1136/bmjopen-2014-005627 (2014).
932	35	Chen, P.-L. *et al.* XRCC1, but not APE1 and hOGG1 gene polymorphisms is a risk factor
933		for pterygium. (2010).
934	36	Taylor, J. C. *et al.* Factors influencing success of clinical genome sequencing across a broad
935		spectrum of disorders. **47**, 717-726, doi:10.1038/ng.3304 (2015).
936	37	Nesbit, M. A. *et al.* Mutations in AP2S1 cause familial hypocalciuric hypercalcemia type 3.
937		*Nature genetics* **45**, 93-97 (2013).
938	38	Robert, X. & Gouet, P. Deciphering key features in protein structures with the new
939		ENDscript server. *Nucleic acids research* **42**, W320-W324 (2014).
940	39	Untergasser, A. *et al.* Primer3—new capabilities and interfaces. *Nucleic acids research* **40**,
941		e115-e115 (2012).
942	40	Moore, J. E. *et al.* Effect of tear hyperosmolarity and signs of clinical ocular surface
943		pathology upon conjunctival goblet cell function in the human ocular surface. *Investigative*
944		*ophthalmology & visual science* **52**, 6174-6180, doi:10.1167/iovs.10-7022 (2011).

945 41   Nesbitt, H. *et al.* Nitric Oxide Up-Regulates RUNX2 in LNCaP Prostate Tumours:
946   Implications for Tumour Growth In Vitro and In Vivo. *Journal of cellular physiology* **231**,
947   473-482 (2016).
948 42   Schmittgen, T. D. & Livak, K. J. Analyzing real-time PCR data by the comparative CT
949   method. *Nature protocols* **3**, 1101-1108 (2008).
950 43   Kulkarni, B., Mohammed, I., Hopkinson, A. & Dua, H. S. Validation of endogenous control
951   genes for gene expression studies on human ocular surface epithelium. *PloS one* **6**, e22301,
952   doi:10.1371/journal.pone.0022301 (2011).
953 44   Notara, M. & Daniels, J. T. Characterisation and functional features of a spontaneously
954   immortalised human corneal epithelial cell line with progenitor-like characteristics. *Brain*
955   *Res Bull* **81**, 279-286, doi:10.1016/j.brainresbull.2009.08.009 (2010).
956 45   Wilkinson, L. *et al.* CRIM1 regulates the rate of processing and delivery of bone
957   morphogenetic proteins to the cell surface. *J Biol Chem* **278**, 34181-34188,
958   doi:10.1074/jbc.M301247200 (2003).
959 46   Vinals, F. & Pouyssegur, J. Confluence of vascular endothelial cells induces cell cycle exit
960   by inhibiting p42/p44 mitogen-activated protein kinase activity. *Molecular and cellular*
961   *biology* **19**, 2763-2772 (1999).
962 47   Kaya, A. I. *et al.* Cell contact-dependent functional selectivity of beta2-adrenergic receptor
963   ligands in stimulating cAMP accumulation and extracellular signal-regulated kinase
964   phosphorylation. *The Journal of biological chemistry* **287**, 6362-6374,
965   doi:10.1074/jbc.M111.301820 (2012).
966 48   Moore, J. E. *et al.* Protection of corneal epithelial stem cells prevents ultraviolet A damage
967   during corneal collagen cross-linking treatment for keratoconus. *The British journal of*
968   *ophthalmology* **98**, 270-274, doi:10.1136/bjophthalmol-2013-303816 (2014).
969 49   Allen, E. H. *et al.* Allele-Specific siRNA Silencing for the Common Keratin 12 Founder
970   Mutation in Meesmann Epithelial Corneal DystrophyAllele-Specific siRNA Silencing.
971   *Investigative ophthalmology & visual science* **54**, 494-502 (2013).
972 50   Lovicu, F., Kolle, G., Yamada, T., Little, M. & McAvoy, J. Expression of Crim1 during
973   murine ocular development. *Mechanisms of development* **94**, 261-265 (2000).
974 51   Pennisi, D. J. *et al.* Crim1KST264/KST264 mice display a disruption of the Crim1 gene
975   resulting in perinatal lethality with defects in multiple organ systems. *Developmental*
976   *Dynamics* **236**, 502-511 (2007).
977 52   Beleggia, F. *et al.* CRIM1 haploinsufficiency causes defects in eye development in human
978   and mouse. *Hum Mol Genet* **24**, 2267-2273, doi:10.1093/hmg/ddu744 (2015).
979 53   Hocking, J. C. *et al.* Morphogenetic defects underlie Superior Coloboma, a newly identified
980   closure disorder of the dorsal eye. **14**, e1007246, doi:10.1371/journal.pgen.1007246 (2018).
981 54   Nakashima, Y. *et al.* Inhibition of the proliferation and acceleration of migration of vascular
982   endothelial cells by increased cysteine-rich motor neuron 1. *Biochem Biophys Res Commun*
983   **462**, 215-220, doi:10.1016/j.bbrc.2015.04.118 (2015).
984 55   Eulalio, A. *et al.* Functional screening identifies miRNAs inducing cardiac regeneration.
985   *Nature* **492**, 376-381, doi:10.1038/nature11739 (2012).
986 56   Ferguson, S. W. *et al.* The microRNA regulatory landscape of MSC-derived exosomes: a
987   systems view. *Scientific reports* **8**, 1419 (2018).
988 57   Ponferrada, V. G. *et al.* CRIM1 complexes with ss-catenin and cadherins, stabilizes cell-cell
989   junctions and is critical for neural morphogenesis. *PloS one* **7**, e32635,
990   doi:10.1371/journal.pone.0032635 (2012).
991 58   Zhang, Y. *et al.* Crim1 regulates integrin signaling in murine lens development.
992   *Development*, doi:10.1242/dev.125591 (2015).
993 59   Zeng, H. *et al.* CRIM1, a newfound cancer-related player, regulates the adhesion and
994   migration of lung cancer cells. *Growth factors (Chur, Switzerland)* **33**, 384-392,
995   doi:10.3109/08977194.2015.1119132 (2015).

996	60	Fan, J. *et al.* Crim1 maintains retinal vascular stability during development by regulating
997		endothelial cell Vegfa autocrine signaling. *Development* **141**, 448-459 (2014).
998	61	Glienke, J., Sturz, A., Menrad, A. & Thierauch, K. H. CRIM1 is involved in endothelial cell
999		capillary formation in vitro and is expressed in blood vessels in vivo. *Mech Dev* **119**, 165-
1000		175 (2002).
1001	62	Wilkinson, L. *et al.* Crim1KST264/KST264 mice implicate Crim1 in the regulation of
1002		vascular endothelial growth factor-A activity during glomerular vascular development. *J Am*
1003		*Soc Nephrol* **18**, 1697-1708, doi:10.1681/asn.2006091012 (2007).
1004	63	Pausch, H. *et al.* Identification of QTL for UV-protective eye area pigmentation in cattle by
1005		progeny phenotyping and genome-wide association analysis. *PLoS One* **7**, e36346,
1006		doi:10.1371/journal.pone.0036346 (2012).
1007	64	Gerber, T. *et al.* Mapping heterogeneity in patient-derived melanoma cultures by single-cell
1008		RNA-seq. *Oncotarget* (2016).
1009	65	Kolle, G., Georgas, K., Holmes, G. P., Little, M. H. & Yamada, T. CRIM1, a novel gene
1010		encoding a cysteine-rich repeat protein, is developmentally regulated and implicated in
1011		vertebrate CNS development and organogenesis. *Mechanisms of development* **90**, 181-193
1012		(2000).
1013	66	O'Leary, J. M. *et al.* Solution structure and dynamics of a prototypical chordin-like cysteine-
1014		rich repeat (von Willebrand Factor type C module) from collagen IIA. *The Journal of*
1015		*biological chemistry* **279**, 53857-53866, doi:10.1074/jbc.M409225200 (2004).
1016	67	Kinna, G. *et al.* Knockdown of zebrafish crim1 results in a bent tail phenotype with defects
1017		in somite and vascular development. *Mechanisms of development* **123**, 277-287 (2006).
1018	68	Kria, L., Ohira, A. & Amemiya, T. Immunohistochemical localization of basic fibroblast
1019		growth factor, platelet derived growth factor, transforming growth factor-beta and tumor
1020		necrosis factor-alpha in the pterygium. *Acta Histochem* **98**, 195-201 (1996).
1021	69	Wu, M. *et al.* Overexpression of low-density lipoprotein receptors stimulated by vascular
1022		endothelial growth factor in fibroblasts from pterygium. *Biomed Pharmacother* **93**, 609-615,
1023		doi:10.1016/j.biopha.2017.06.090 (2017).
1024	70	Chui, J. *et al.* Ophthalmic pterygium: a stem cell disorder with premalignant features. *Am J*
1025		*Pathol* **178**, 817-827, doi:10.1016/j.ajpath.2010.10.037 (2011).
1026	71	Dushku, N. & Reid, T. W. Immunohistochemical evidence that human pterygia originate
1027		from an invasion of vimentin-expressing altered limbal epithelial basal cells. *Curr Eye Res*
1028		**13**, 473-481 (1994).
1029	72	Gebhardt, M. *et al.* Differential expression of vascular endothelial growth factor implies the
1030		limbal origin of pterygia. *Ophthalmology* **112**, 1023-1030,
1031		doi:10.1016/j.ophtha.2005.01.023 (2005).
1032	73	Wilkinson, L. *et al.* Crim1KST264/KST264 mice implicate Crim1 in the regulation of
1033		vascular endothelial growth factor-A activity during glomerular vascular development.
1034		*Journal of the American Society of Nephrology* **18**, 1697-1708 (2007).
1035	74	Marionnet, C., Tricaud, C. & Bernerd, F. Exposure to non-extreme solar UV daylight:
1036		spectral characterization, effects on skin and photoprotection. *International journal of*
1037		*molecular sciences* **16**, 68-90 (2014).
1038	75	Courtney, D. G. *et al.* siRNA silencing of the mutant keratin 12 allele in corneal limbal
1039		epithelial cells grown from patients with Meesmann's epithelial corneal dystrophy. *Invest*
1040		*Ophthalmol Vis Sci* **55**, 3352-3360, doi:10.1167/iovs.13-12957 (2014).
1041	76	Cagnol, S. & Chambard, J. C. ERK and cell death: mechanisms of ERK-induced cell death--
1042		apoptosis, autophagy and senescence. *The FEBS journal* **277**, 2-21, doi:10.1111/j.1742-
1043		4658.2009.07366.x (2010).
1044	77	Liang, K. *et al.* Expression of cell proliferation and apoptosis biomarkers in pterygia and
1045		normal conjunctiva. (2011).

1046 78 Kwok, L. S. & Coroneo, M. T. A model for pterygium formation. *Cornea* **13**, 219-224
1047   (1994).
1048 79 Nakashima, Y. & Takahashi, S. Induction of cysteine-rich motor neuron 1 mRNA
1049   expression in vascular endothelial cells. *Biochemical and biophysical research*
1050   *communications* **451**, 235-238, doi:10.1016/j.bbrc.2014.07.108 (2014).
1051 80 Kannabiran, C. & Klintworth, G. K. TGFBI gene mutations in corneal dystrophies. *Human*
1052   *mutation* **27**, 615-625 (2006).
1053 81 Tan, D. T., Tang, W. Y., Liu, Y. P., Goh, H. S. & Smith, D. R. Apoptosis and apoptosis
1054   related gene expression in normal conjunctiva and pterygium. *The British journal of*
1055   *ophthalmology* **84**, 212-216 (2000).
1056 82 Mencucci, R. *et al.* Effects of riboflavin/UVA corneal cross-linking on keratocytes and
1057   collagen fibres in human cornea. *Clinical & experimental ophthalmology* **38**, 49-56 (2010).
1058 83 Buron, N. *et al.* Differential mechanisms of conjunctival cell death induction by ultraviolet
1059   irradiation and benzalkonium chloride. *Investigative ophthalmology & visual science* **47**,
1060   4221-4230 (2006).
1061 84 Yam, J. C. & Kwok, A. K. Ultraviolet light and ocular diseases. *International*
1062   *ophthalmology* **34**, 383-400 (2014).
1063 85 Cullen, A. P. Photokeratitis and other phototoxic effects on the cornea and conjunctiva.
1064   *International journal of toxicology* **21**, 455-464 (2002).
1065 86 DILLON, J., Zheng, L., MERRIAM, J. C. & GAILLARD, E. R. The optical properties of
1066   the anterior segment of the eye: implications for cortical cataract. *Experimental eye research*
1067   **68**, 785-795 (1999).
1068 87 Newton, R., Reeves, G., Beral, V., Ferlay, J. & Parkin, D. Effect of ambient solar ultraviolet
1069   radiation on incidence of squamous-cell carcinoma of the eye. *The Lancet* **347**, 1450-1451
1070   (1996).
1071 88 Lucas, R. M., McMichael, A. J., Armstrong, B. K. & Smith, W. T. Estimating the global
1072   disease burden due to ultraviolet radiation exposure. *International journal of epidemiology*
1073   **37**, 654-667 (2008).
1074 89 Hirst, L. W. Distribution, risk factors, and epidemiology of pterygium. *Pterygium, Kugler*
1075   *Publications, The Hague, The Netherlands*, 15-27 (2000).
1076 90 Raghunath, A. & Perumal, E. Micro-RNAs and their roles in eye disorders. *Ophthalmic*
1077   *research* **53**, 169-186, doi:10.1159/000371853 (2015).
1078 91 Tam, O. H. *et al.* Crim1 is required for maintenance of the ocular lens epithelium.
1079   *Experimental eye research* **170**, 58-66, doi:10.1016/j.exer.2018.02.012 (2018).
1080 92 Machens, A. *et al.* Age-related penetrance of endocrine tumours in multiple endocrine
1081   neoplasia type 1 (MEN1): a multicentre study of 258 gene carriers. *Clinical endocrinology*
1082   **67**, 613-622 (2007).
1083 93 Vitt, U. A., Hsu, S. Y. & Hsueh, A. J. Evolution and classification of cystine knot-
1084   containing hormones and related extracellular signaling molecules. *Molecular*
1085   *endocrinology* **15**, 681-694 (2001).
1086 94 Pearton, D. J., Ferraris, C. & Dhouailly, D. Transdifferentiation of corneal epithelium:
1087   evidence for a linkage between the segregation of epidermal stem cells and the induction of
1088   hair follicles during embryogenesis. *The International journal of developmental biology* **48**,
1089   197-201, doi:10.1387/ijdb.031744dp (2004).
1090 95 Engelsvold, D. H. *et al.* miRNA and mRNA expression profiling identifies members of the
1091   miR-200 family as potential regulators of epithelial-mesenchymal transition in pterygium.
1092   *Exp Eye Res* **115**, 189-198, doi:10.1016/j.exer.2013.07.003 (2013).
1093 96 Watson, S. *et al.* Limbal dermoid epithelium shares phenotypic characteristics common to
1094   both hair epidermal and limbal epithelial stem cells. *Current eye research* **38**, 835-842,
1095   doi:10.3109/02713683.2013.780625 (2013).

1096 97   He, Y.-Y., Council, S. E., Feng, L. & Chignell, C. F. UVA-induced cell cycle progression is
1097   mediated by a disintegrin and metalloprotease/epidermal growth factor receptor/AKT/Cyclin
1098   D1 pathways in keratinocytes. *Cancer research* **68**, 3752-3758 (2008).
1099 98   Assefa, Z., Van Laethem, A., Garmyn, M. & Agostinis, P. Ultraviolet radiation-induced
1100   apoptosis in keratinocytes: on the role of cytosolic factors. *Biochimica et Biophysica Acta*
1101   *(BBA)-Reviews on Cancer* **1755**, 90-106 (2005).
1102 99   Moan, J. 7 Visible Light and UV Radiation. *Radiation*, 69 (2001).
1103 100   Tsai, Y. Y. *et al.* Oxidative DNA damage in pterygium. *Molecular vision* **11**, 71-75 (2005).
1104 101   Mercola, M. *et al.* Dominant-negative mutants of a platelet-derived growth factor gene.
1105   *Genes & development* **4**, 2333-2341 (1990).
1106 102   Millauer, B., Shawver, L. K., Plate, K. H., Risaui, W. & Ullrich, A. Glioblastoma growth
1107   inhibited in vivo by a dominant-negative Flk-1 mutant. *Nature* **367**, 576-579 (1994).
1108 103   Casari, C. *et al.* The dominant-negative von Willebrand factor gene deletion p.
1109   P1127_C1948delinsR: molecular mechanism and modulation. *Blood* **116**, 5371-5376
1110   (2010).
1111 104   Castaman, G., Eikenboom, J. C., Missiaglia, E. & Rodeghiero, F. Autosomal dominant type
1112   1 von Willebrand disease due to G3639T mutation (C1130F) in exon 26 of von Willebrand
1113   factor gene: description of five Italian families and evidence for a founder effect. *British*
1114   *journal of haematology* **108**, 876-879 (2000).
1115